Neuropilin-1 promotes cirrhosis of the rodent and human liver by enhancing PDGF/TGF-β signaling in hepatic stellate cells

Sheng Cao,[1] Usman Yaqoob,[1] Amitava Das,[1] Uday Shergill,[1] Kumaravelu Jagavelu,[1] Robert C. Huebert,[1] Chittaranjan Routray,[1] Soha Abdelmoneim,[1] Meher Vasdev,[1] Edward Leof,[2] Michael Charlton,[3] Ryan J. Watts,[4] Debabrata Mukhopadhyay,[2] and Vijay H. Shah[1]

[1]Gastroenterology Research Unit, [2]Department of Biochemistry and Molecular Biology, and [3]Department of Internal Medicine, Mayo Clinic, Rochester, Minnesota, USA. [4]Department of Neuroscience, Genentech, Inc., South San Francisco, California, USA.

PDGF-dependent hepatic stellate cell (HSC) recruitment is an essential step in liver fibrosis and the sinusoidal vascular changes that accompany this process. However, the mechanisms that regulate PDGF signaling remain incompletely defined. Here, we found that in two rat models of liver fibrosis, the axonal guidance molecule neuropilin-1 (NRP-1) was upregulated in activated HSCs, which exhibit the highly motile myofibroblast phenotype. Additionally, NRP-1 colocalized with PDGF-receptor β (PDGFRβ) in HSCs both in the injury models and in human and rat HSC cell lines. In human HSCs, siRNA-mediated knockdown of NRP-1 attenuated PDGF-induced chemotaxis, while NRP-1 overexpression increased cell motility and TGF-β–dependent collagen production. Similarly, mouse HSCs genetically modified to lack NRP-1 displayed reduced motility in response to PDGF treatment. Immunoprecipitation and biochemical binding studies revealed that NRP-1 increased PDGF binding affinity for PDGFRβ-expressing cells and promoted downstream signaling. An NRP-1 neutralizing Ab ameliorated recruitment of HSCs, blocked liver fibrosis in a rat model of liver injury, and also attenuated VEGF responses in cultured liver endothelial cells. In addition, NRP-1 overexpression was observed in human specimens of liver cirrhosis caused by both hepatitis C and steatohepatitis. These studies reveal a role for NRP-1 as a modulator of multiple growth factor targets that regulate liver fibrosis and the vascular changes that accompany it and may have broad implications for liver cirrhosis and myofibroblast biology in a variety of other organ systems and disease conditions.

Introduction

Liver cirrhosis is characterized by excessive extracellular matrix deposition that leads to a dense network of scar tissue that encases nodules of hepatocyte parenchyma and is associated with prominent derangements in hepatic sinusoidal vascular structure (1). This in turn leads to profound hepatic and systemic hemodynamic alterations in portal hypertension and eventually to severe clinical complications (2). Current paradigms suggest a key role for the hepatic stellate cell (HSC) in liver cirrhosis by virtue of the activation of a quiescent vascular pericyte-like cell into a myofibroblastic cell that is characterized by a phenotypic constellation that includes enhanced proliferation, motility, and ability to deposit extracellular matrix (3, 4). Interestingly, an increasing body of recent studies has revealed an important contribution of pericytes and their motility to angiogenesis and vascular remodeling (5). These vascular functions of pericytes have in turn been intimately linked to fibrosis and cirrhosis (6). These existing paradigms have stimulated studies that aim for a more informed understanding of the mechanisms of HSC motility and migration that are required for these pathobiological processes to occur.

The canonical pathway that promotes motility, migration, and recruitment of HSCs is the binding of PDGF ligand with one of its receptors, PDGFRβ (7–9). PDGFRβ is a transmembrane 180-kDa glycoprotein with intrinsic protein tyrosine kinase activity and is expressed on cells of mesenchymal origin, including smooth muscle cells and pericytes (7–9). Indeed, deletion of PDGF or PDGFRβ in mice leads to embryonic lethality, owing to leaky and hemorrhagic vessels that lack vascular pericytes (10–12). Previous work has identified the enhanced activation of the PDGF/PDGFRβ pathway as a key factor in the conversion of HSCs into myofibroblasts and the ensuing recruitment of these cells to sites of sinusoidal remodeling and matrix deposition (5, 13–15). However, the mechanisms that confer enhanced activation of the PDGF/PDGFRβ axis remain incompletely understood, a gap in knowledge that is particularly important to fill owing to the therapeutic opportunities that could be uncovered by modulating this pathway for treatment of liver cirrhosis in humans.

In the present study, we sought to identify new mechanisms that may regulate the PDGF/PDGFRβ pathway in HSCs and to explore their pathobiological significance in the process of liver cirrhosis. Our work reveals a role of the neuronal growth cone molecule and VEGF coreceptor protein neuropilin-1 (NRP-1) (16) in this process. NRP-1 protein levels are increased in HSCs from complementary models of liver cirrhosis in a temporal and spatial pattern that parallels PDGFRβ. We demonstrate that NRP-1 promotes PDGFRβ migration signaling, which is mechanistically achieved by enhancing PDGF ligand binding with HSCs and relaying the PDGFRβ phosphorylation signal selectively toward the small GTPase Rac1. This selectivity is achieved through routing of signals through the non-receptor tyrosine kinase protein c-Abl (17). NRP-1 also promotes signaling of other growth factors

Authorship note: Sheng Cao, Usman Yaqoob, and Amitava Das contributed equally to this work.

Conflict of interest: R.J. Watts is an employee of Genentech.

Citation for this article: *J Clin Invest.* 2010;120(7):2379–2394. doi:10.1172/JCI41203.

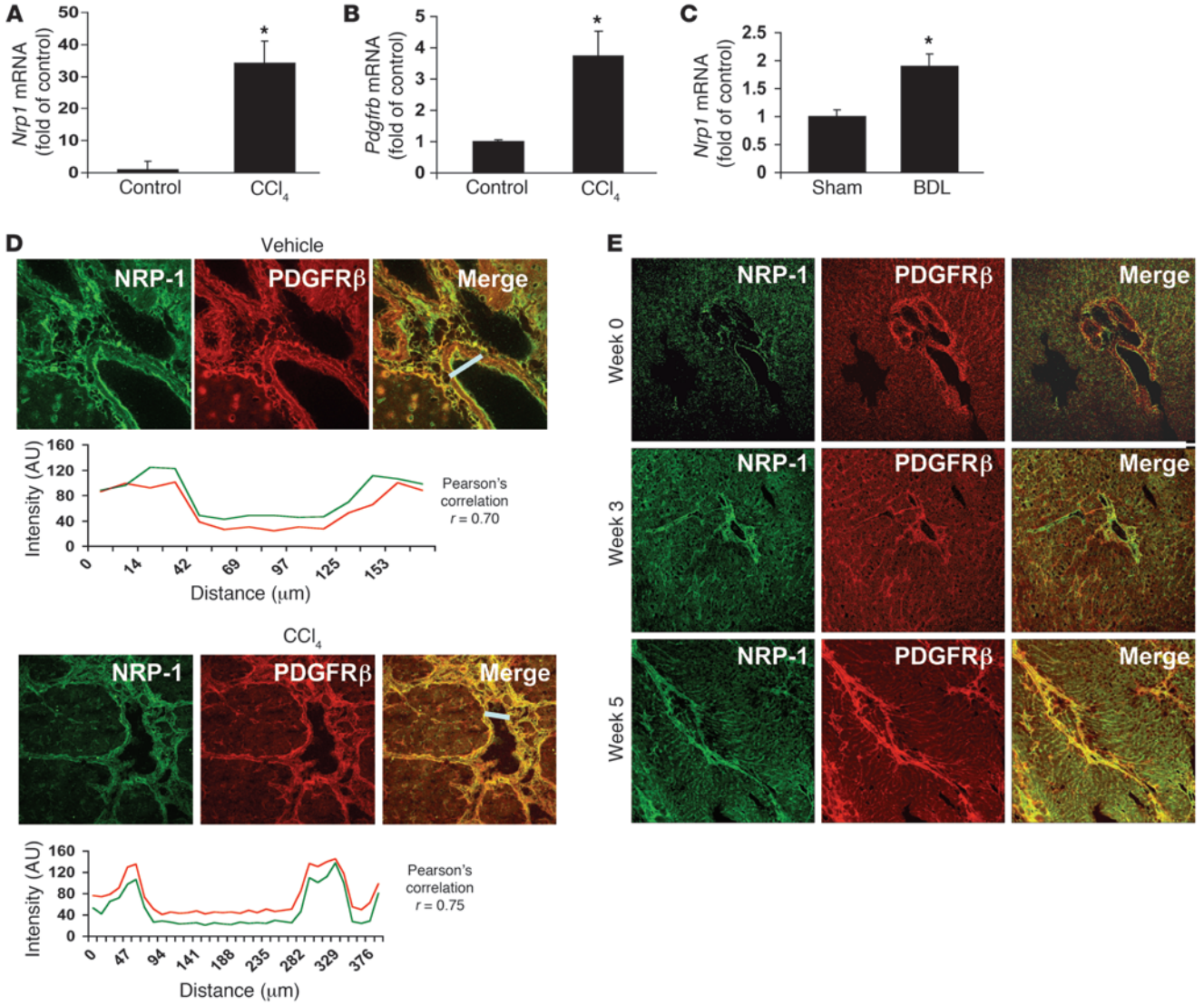

Figure 1

NRP-1 expression correlates with activation of HSCs into a motile myofibroblastic phenotype. (**A** and **B**) *Nrp1* and *Pdgfrb* mRNA levels in isolated rHSCs from CCl_4-treated rats were increased compared with those from control rats as measured using qRT-PCR ($n = 3$, $^*P < 0.05$). (**C**) *Nrp1* mRNA levels were increased in rHSCs from BDL as compared with sham-operated rats ($n = 5$, $^*P < 0.05$). (**D**) Five-micrometer sections of rat liver were stained with an Ab against NRP-1 (green). Liver tissues of rats treated with either vehicle or CCl_4 were coimmunostained for PDGFRβ and NRP-1. Representative images for NRP-1 staining (in green) are shown in the left panels and for PDGFRβ (in red), in the middle panels; overlays of the two (in yellow) are in the right panels. Below each image is the colocalization analysis for each of the overlay images. The graph peaks represent the fluorescence intensities of the staining at the given distances (in micrometers) along the straight white bar. The white bars in the overlay images represent the area selected for colocalization. (**E**) Time course expression of NRP-1 in liver of CCl_4-treated rats. Liver tissue of rats treated with CCl_4 was sectioned at various time points and coimmunostained using NRP-1 and PDGFRβ Ab. Original magnification, ×10.

important in the development of liver cirrhosis, including TGF-β and VEGF. Furthermore, a recently characterized NRP-1 neutralizing Ab (18) protects animals from liver cirrhosis by regulating not only PDGF-dependent HSC motility but also collagen deposition and angiogenesis. Importantly, these mechanistic observations are applicable to humans, as we demonstrated that NRP-1 expression in HSCs correlates with the severity of fibrosis in two common causes of fibrosis, nonalcoholic steatohepatitis (NASH) and hepatitis C. Thus, these complementary in vitro and in vivo studies define a mechanistic role for NRP-1 in the enhanced migration of HSCs in liver cirrhosis and identify NRP-1 as a target for clinical therapeutics by virtue of its ability to regulate a relevant array of growth factor molecules implicated in myofibroblast activation.

Results

As an initial step to identify new molecular targets that regulate motility of HSCs, we reviewed recent comprehensive microarray analyses that identified genes that were upregulated in activated HSCs (19), which take on a highly motile, myofibroblastic phenotype, as occurs in liver injury and fibrosis models such as chronic

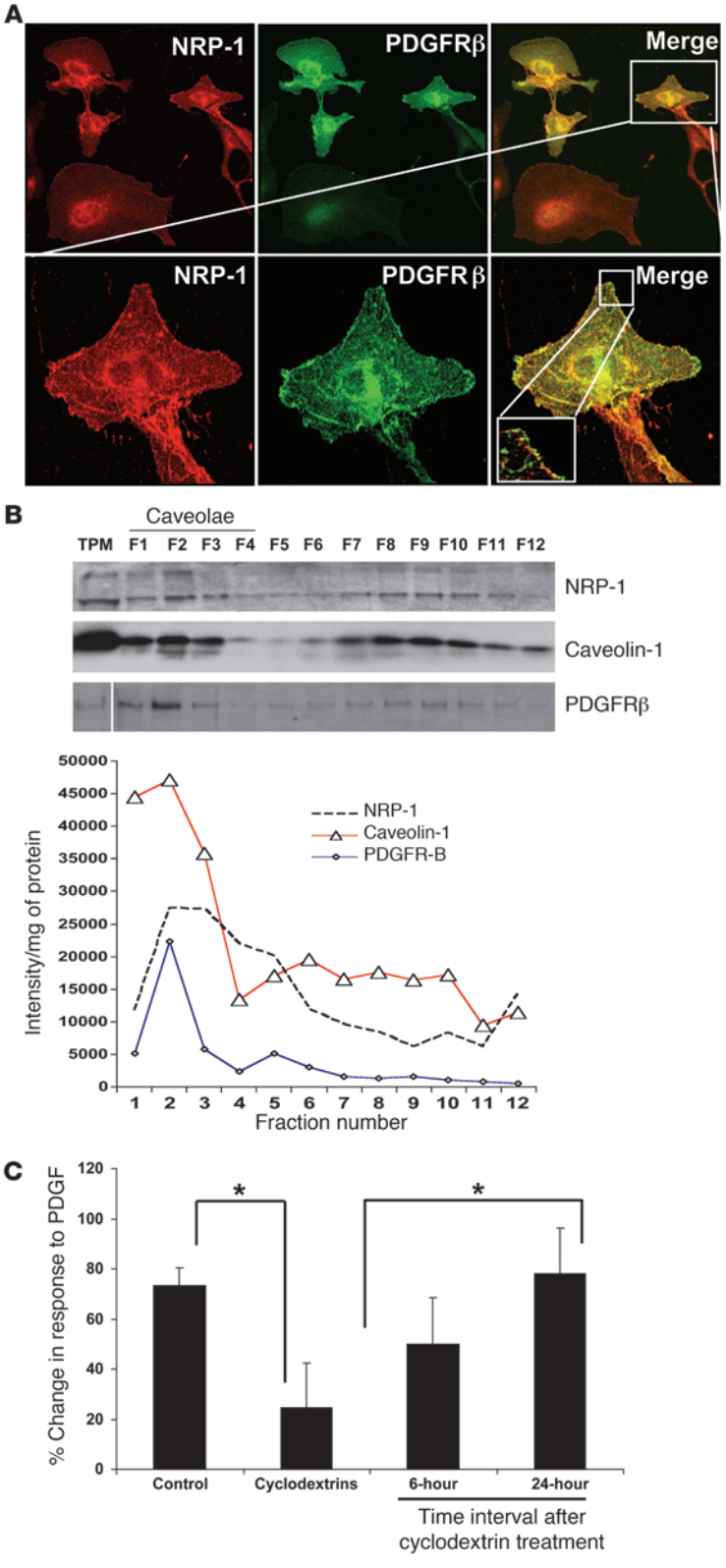

Figure 2
NRP-1 is enriched within low-buoyant-density membrane microdomains and colocalizes with PDGFRβ. (**A**) LX2 cells transduced with PDGFRβ retrovirus were cotransduced with Ad-NRP-1–RFP. Cells were immunostained with NRP-1 (red) and PDGFRβ (green) Abs and photographed under a confocal microscope. The top row shows ×20 magnification and the bottom row shows ×63 magnification of the cropped cell, with further magnification of the cropped area (representative photomicrographs or Western blot are from 3 independent experiments). (**B**) HSC lysates were prepared for sucrose density gradient fractionation studies, and equal volumes of each fraction were analyzed by SDS-PAGE (top). White line indicates splicing of a noncontiguous sample from the same membrane. NRP-1 was also found to be enriched within low-buoyant-density fractions as assessed by levels of NRP-1 per microgram protein within each fraction when SDS-PAGE fraction signal was normalized for protein concentration (bottom). Separation and purity of membrane fractions were determined by immunoblotting for caveolin-1, a marker for low-buoyant-density membranes ($n = 3$). TPM, total plasma membrane. (**C**) Cyclodextrin, a compound that disrupts low-buoyant-density vesicle formation, inhibits PDGF-dependent hHSC chemotaxis. Cyclodextrin inhibition of PDGF-induced HSC chemokinesis was studied using time-lapse video microscopy followed by analysis using MetaMorph Imaging software. The right 2 bars show a reversible effect of cyclodextrin, thus reducing the likelihood of cell toxicity relating to the compound ($n = 3$, $^*P < 0.05$).

administration of carbon tetrachloride (CCl_4) or bile duct ligation (BDL) (20). This approach, confirmed by our own focused microarray analyses (data not shown), quantitative RT-PCR (qRT-PCR), and Western blot analysis, led us to identify expression of the semaphorin-binding protein and regulator of neuronal growth cone collapse NRP-1 (16) as a molecular target that is upregulated in conjunction with PDGFR in activated HSCs isolated from CCL_4 or BDL rats with liver injury and fibrosis (Figures 1, A–C). Further analysis of the spatial localization of NRP-1 within HSCs in situ confirmed that NRP-1 is colocalized with PDGFR and upregulated in a temporal relationship with HSC activation in such in vivo models, especially within fibrous septa (Figures 1, D and E). Interestingly, NRP-1–positive HSCs in situ also corresponded to varying degrees with α-SMA–, desmin-, and NG2-positive HSC populations residing within sinusoids and fibrous septa (see Supplemental Figures 1, A–C; supplemental material available online with this article; doi:10.1172/JCI41203DS1). However, of these markers, the closest interposition of NRP-1 positivity was observed with HSCs expressing PDGFRβ (Pearson coefficient, 0.7–0.75; Figure 1D). From a subcellular perspective, colocalization of NRP-1 and PDGFRβ was observed within distinct microdomains of plasma membrane (Figure 2A) within the LX2 HSC. LX2 HSCs are immortalized HSCs with a myofibroblast-like phenotype (21) that were used in some experiments along with HSCs from rats and HSCs from humans. Although all are referred to as HSCs in Results, each cell type is specifically indicated within each respective figure legend. The distinct microdomains of plasma membrane were revealed to be of a low-buoyant-density nature consistent with caveolae based on more detailed sucrose-based subcellular fractionation techniques (Figure 2B; see membrane fractions F1–F3, which are enriched in NRP-1, PDGFRβ, and the caveolae marker caveolin) (22). Spatial distribution of NRP-1 with PDGFRβ is likely important, since

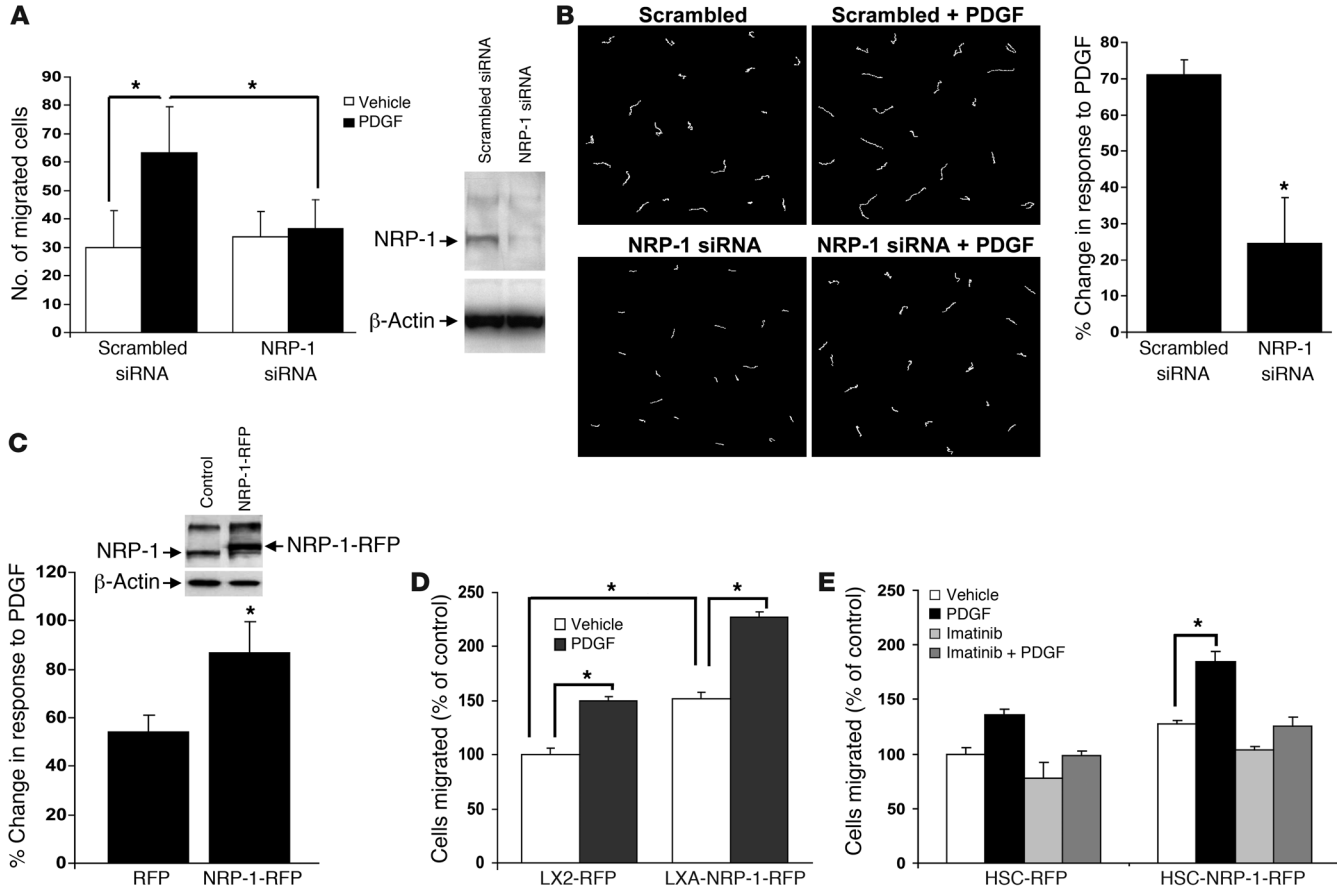

Figure 3

NRP-1 is required for PDGF-dependent HSC motility and chemotaxis. hHSCs were transfected with NRP-1 siRNA or a scrambled siRNA. Cells were prepared for analysis of cell movement by plating in a Boyden chamber for analysis of cell chemotaxis (**A**) or alternatively for individual cell motility by using DIC imaging and MetaMorph software (**B**). (**A**) hHSCs transfected with NRP-1 siRNA evidenced diminished PDGF-dependent cell motility as assessed by measurement of distance traveled and also evidenced impaired chemotactic responses to PDGF ($n = 4$, $^*P < 0.05$). NRP-1 protein knockdown by NRP-1 siRNA is depicted in the right-side Western blot. (**B**) Representative examples of migration tracks of cells transfected with Cy3-labeled NRP-1 siRNA or scrambled siRNA and tracked for 3 hours. Cell movements were recorded by time-lapse videomicroscopy and quantified by MetaMorph software. Total distance covered by the tracked cells was measured and plotted as percentage of change in response to PDGF ($n = 3$, $^*P < 0.05$). (**C**) hHSCs were transduced with retroviral vector encoding RFP-tagged NRP-1 (NRP-1–RFP) or, alternatively, RFP alone, and NRP-1–RFP overexpression was assessed by Western blot analysis. Cells were analyzed for cell motility using a wounding assay with tracking of fluorescent signal of individual cells ($n = 3$, $^*P < 0.05$). (**D**) Cell migration was also studied using a Boyden chamber in LX2 cells transduced with RFP alone and NRP-1–RFP retrovirus. Cells transduced with NRP-1–RFP evidenced enhanced PDGF-dependent cell movement as compared with cells transduced with RFP control. Quantification of data in terms of percent change in motility is shown ($n = 3$, $^*P < 0.05$). (**E**) Imatinib, a pharmacologic inhibitor of PDGFRβ, blocked the enhanced migration conferred by NRP-1–RFP overexpression ($n = 3$, $^*P < 0.05$).

real-time video microscopy demonstrated that PDGF-induced LX2 chemokinesis is inhibited by cyclodextrin (23), a compound that disrupts caveolae membranes (Figure 2C). These results support the potential pathobiologic significance of NRP-1 in HSCs based on upregulation of its expression in disease conditions and codistribution with PDGFRβ, a canonical target for HSC vascular function. We exploited these observations in greater detail by exploring a potential signaling crosstalk between these two molecules, as described below.

We used complementary gain- and loss-of-function approaches in combination with various assays to measure cell motility and migration to decipher the effects of NRP-1 on HSC movement. While PDGF increased HSC chemotaxis, siRNA knockdown of NRP-1 inhibited PDGF-induced chemotaxis (Figure 3A). These results were corroborated in the context of chemokinesis as well, using real-time video microscopy, in which NRP-1 siRNA attenuated PDGF-induced chemokinesis of HSCs (Figure 3B). Furthermore, overexpression of NRP-1 in HSCs using a red fluorescence protein–tagged (RFP-tagged) retroviral delivery system showed a significant increase in motility as compared with control cells transfected with RFP alone in the complementary wounding assay (24) (Figure 3C). NRP-1–RFP–positive cells also showed a significant increase in PDGF dependent cell motility, indicating that NRP-1 is sufficient for enhancing PDGF-dependent cell migration, thus further substantiating this observation (Figure 3D). NRP-1–RFP cells did evidence a modestly increased cell prolifera-

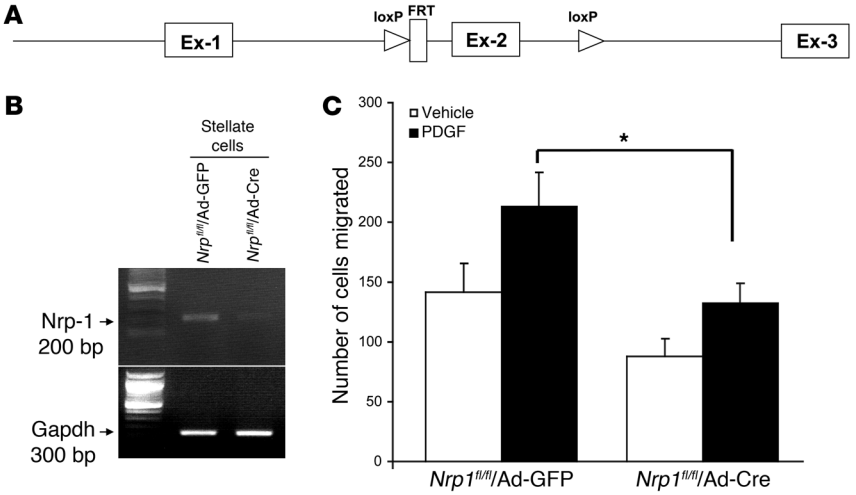

Figure 4
Migration is reduced in HSCs isolated from mice with genetic deletion of NRP-1. (**A**) Strategy for the deletion on NRP-1. The targeted allele *Nrp1* within exon 2 (Ex-2) is flanked with loxP sites (triangles). Cre-recombinase under the control of the adenovirus CMV promoter mediates the excision of loxP-flanked exon 2. (**B**) Assessment of *Nrp1* deletion using adenovirus Cre in HSCs; Cre-mediated excision on the lox-flanked exon 2 leads to loss of amplified PCR fragment of 200 bp. (**C**) The migration response to PDGF in HSCs isolated from NRP-1 floxed mice transduced with AdCre is reduced compared with cells transduced with AdGFP as measured by Boyden chamber assay (*$P < 0.05$ compared with AdGFP).

tion rate (from 0.49 ± 0.017 [RFP] to 0.81 ± 0.014 [NRP-1–RFP]) of about 1.65-fold after 48 hours; however, this was unlikely to have confounded the chemotactic studies, which were performed in a 4-hour window. Recent studies have demonstrated varying crosstalk between VEGF receptor 2 (KDR) and the PDGF system in smooth muscle cells and pericytes (25–27). Importantly, the cells used in this experiment did not express KDR at a level detectable by our own Western blot conditions, nor did they generate canonical signal transduction activation in response to VEGF ligand or a chemotactic response to other NRP-1 ligands, including Sema 3a (see Supplemental Figure 2, A–F), thus reducing the likelihood that NRP-1 was functioning through these alternative mechanisms in our specific experimental setting. Furthermore, NRP-1 overexpression did not promote cell motility in cells treated with the PDGFRβ antagonist imatinib (17), indicating that the mechanism of action by which NRP-1 enhances cell motility requires PDGFRβ (Figure 3E). Last, since imatinib may also inhibit molecular targets downstream of and parallel to PDGFRβ (17), we also repeated these studies using PDGFRβ siRNA, which blocked cell migration despite the presence of endogenous NRP-1 (Supplemental Figure 4A). However, NRP-1 did regulate FGF-induced HSC migration (Supplemental Figure 4B), suggesting to us that NRP-1 may promote multiple cirrhosis–related growth factor pathways in HSCs, a concept that was pursued in greater depth in the context of TGF-β, as discussed further below.

Next, we used a genetic *Nrp1*-knockout approach to test our hypothesis. This was achieved by isolating HSCs from mice in which exon 2 of *Nrp1* was floxed by LoxP sites (28) (Figure 4A) and transducing cells with adenovirus Cre (Figure 4B). HSCs transduced with adenovirus Cre showed less migration in response to PDGF as compared with cells transduced with adenovirus GFP (Figure 4C). These results in total indicate an integral role for NRP-1 in the process of PDGF-mediated primary cultured HSC motility, thus spawning a series of mechanistic studies that are described below.

NRP-1 has been proposed as a "coreceptor," although this concept is controversial, especially with regard to whether coreceptor function is achieved by virtue of NRP-1 regulation of receptor-ligand binding or alternatively through a distinct intracellular mechanism of regulating signal transduction downstream of the primary receptor (29, 30). In order to investigate how NRP-1 regulates PDGFRβ, we performed binding studies in these cells in vitro, to determine whether NRP-1 binds PDGF ligand directly or alternatively by enhancing PDGF ligand binding with the PDGF receptor. Binding studies using ^{125}I-PDGF labeling revealed that PDGF binding is enhanced in cells overexpressing NRP-1 (Figure 5B versus Figure 5A) and that this was reduced in the presence of a cold competitor (Supplemental Figure 5A). Scatchard analysis revealed that PDGF-PDGFRβ interaction occurred at high affinity, with a K_d of 193 pM (Figure 5B) with overexpression of NRP-1, compared with a K_d of 606 pM in control cells (Figure 5A). Conversely, when NRP-1 was knocked down by a specific siRNA, the binding of ^{125}I-PDGF to cells was markedly decreased (Supplemental Figure 5B), indicating that NRP-1 enhances PDGF binding with HSCs. To further extend these findings, we performed cross-linking and immunoprecipitation of PDGFRβ from cells incubated with ^{125}I-PDGF and then performed autoradiography of SDS-PAGE–separated proteins. The autoradiography data showed that the binding of PDGF to PDGFRβ markedly increased when NRP-1 was overexpressed in these cells (Figure 5C). In parallel experiments, immunoprecipitation of NRP-1 under basal conditions detected only negligible levels of PDGF ligand, although further coprecipitation was detected when cells overexpressed NRP-1 (Figure 5C). Thus, these results indicate that NRP-1 facilitates PDGF ligand binding to cells predominantly, although not exclusively, through increased binding with PDGFRβ.

We next sought to determine whether NRP-1 could directly promote PDGF-dependent signal transduction. First, we determined the influence of NRP-1 on PDGFRβ autophosphorylation of a conserved tyrosine residue within the kinase domain (Tyr857 of the PDGFRβ), which is a key indicator of receptor activity (31). As shown in Figure 6A, overexpression of NRP-1 in HSCs increased the intensity and duration of PDGFRβ autophosphorylation on Tyr857 by 5-fold as assessed by quantitation of the depicted Western blot. However, the canonical downstream effectors for PDGFRβ-dependent proliferation such as Akt and ERK, though phosphorylated in response to PDGF, were not influenced by changes in cellular levels of NRP-1 (Figure 6A). Conversely, PDGFRβ activation of Rac1, which promotes migration, was prominently increased, by 2- to 3-fold, at all studied time points in cells overexpressing NRP-1 (Figure 6B). Additionally, retroviral overexpression of a dominant negative form of Rac1 (Rac1DN) blocked the increase in migration conferred by NRP-1 overexpres-

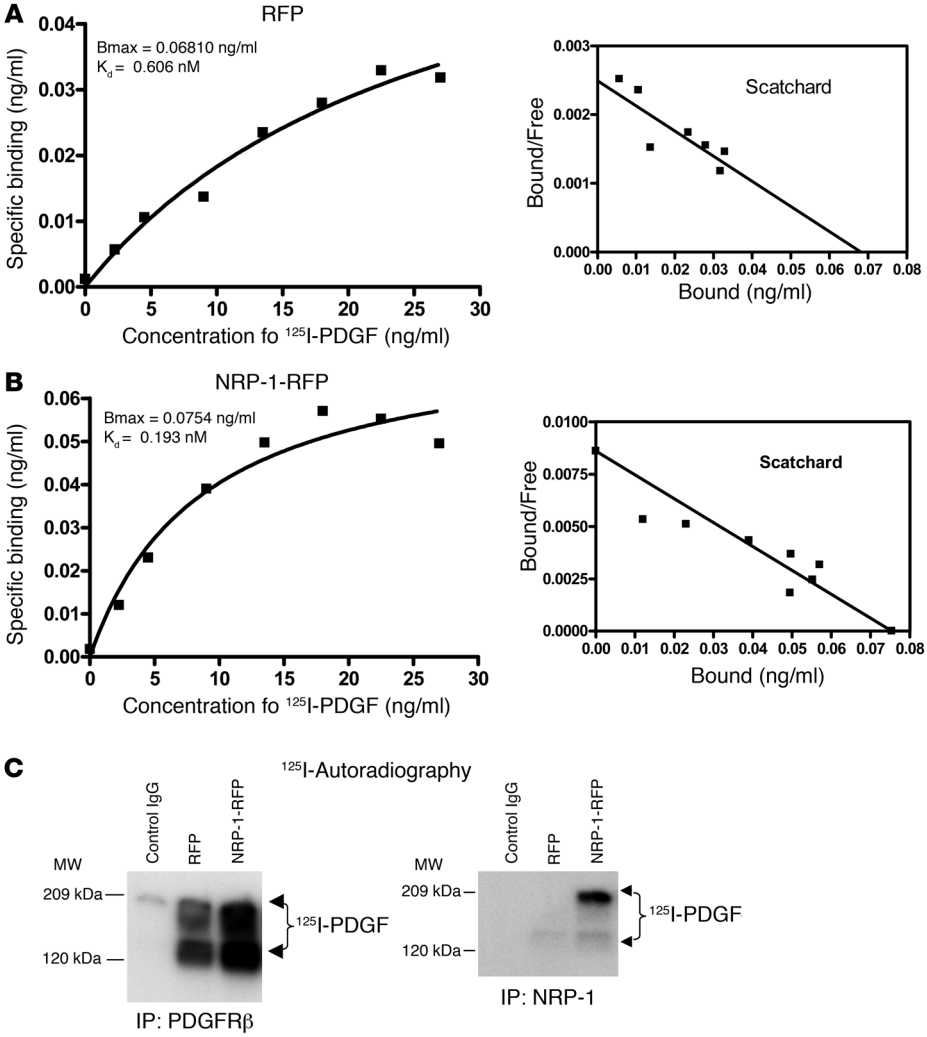

Figure 5
NRP-1 enhances cellular binding of PDGF ligand. (**A** and **B**) PDGF was labeled with ^{125}I and incubated with hHSCs at varying concentrations; binding curves were generated and respective dissociation constants were calculated. NRP-1–overexpressing cells showed high affinity for PDGF (**B**), with K_d of 193 pM compared with K_d of 606 pM in the control RFP-transfected hHSCs (**A**). Bmax indicates the amount of PDGF required to saturate the population of PDGF receptors present in the samples. (**C**) Immunoprecipitation of PDGFRβ from cell lysates incubated with ^{125}I-labeled PDGF showed enhanced binding with NRP-1–RFP compared with control RFP (left panel). Immunoprecipitation of NRP-1–RFP from same lysates showed relatively less coprecipitation of PDGFRβ with NRP-1 (right panel).

sion (Figure 6C), indicating that NRP-1 selectively and specifically activates PDGFRβ signals that lead to downstream Rac1 activation and cell migration. Thus, NRP-1 may provide a molecular switch for determining distinct and alternative downstream PDGFRβ signaling pathways (32). Interestingly, PDGFRβ phosphorylation and Rac1 activation were greater in cells overexpressing NRP-1 even in the absence of PDGF ligand (see time 0 in Figure 6, A and B, Western blot with 2-fold increase in NRP-1–overexpressing cells), indicating that intracellular crosstalk between NRP-1 and PDGFRβ may occur even independent of ligand binding.

We next sought to investigate the mechanism by which NRP-1 signals could be preferentially directed towards Rac1. Since recent studies have identified the non-receptor tyrosine kinase c-Abl as a key regulator of Rac1 activity through its ability to phosphorylate and activate the GTPase effector protein SOS-1 (33), we focused on this molecule as a potential link between NRP-1 and Rac1 activation. To pursue this direction in further detail, we performed parallel studies not only in HSC but also in mouse embryonic fibroblasts (MEFs) isolated from mice genetically deficient in c-Abl and its related protein Arg (17). MEFs were used because these mice are embryonic lethal, thus precluding HSC isolation, and MEFs share a number of signaling features with HSCs (17). Indeed, Rac activity was markedly diminished in MEFs isolated from mice genetically deficient in c-Abl (*c-Abl/Arg*$^{-/-}$ mice; Figure 7A) as well as HSCs transfected with c-Abl siRNA (Figure 7B). Furthermore, the increase in Rac1 activity conferred by overexpression of NRP-1 was markedly attenuated in *c-Abl/Arg*$^{-/-}$ MEFs (Figure 7C). We next examined c-Abl kinase activity in response to NRP-1 overexpression. As shown in Figure 7D, PDGF induced c-Abl activity in LX2 cells, as did overexpression of NRP-1, as assessed by phosphorylation of the c-Abl substrate Crk. Concordantly, c-Abl activity was diminished in MEFs isolated from mice genetically deficient in NRP-1 (Figure 7D). Interestingly, coimmunoprecipitation analysis demonstrated that NRP-1 resides in a complex with c-Abl in cells overexpressing NRP-1, as well as in cells stimulated with PDGF, while this association was diminished in *c-Abl* and *Nrp1*-knockout cells (Figure 7E). NRP-1 overexpression was not associated with phosphorylation of the p85 subunit of PI3K, which is situated upstream from Akt (Supplemental Figure 7), further supporting signal selectivity of NRP-1 toward Rac1 rather than Akt. Thus, these studies support a role for c-Abl as a molecule that directs NRP-1/PDGFR signals toward Rac1.

A recently characterized series of NRP-1 Abs have been used to block NRP-1 function in vitro and in vivo (18). With the goal of using this tool to decipher the role of NRP-1 in liver cirrhosis in vivo, we next examined the Abs' function in chemotaxis assays on

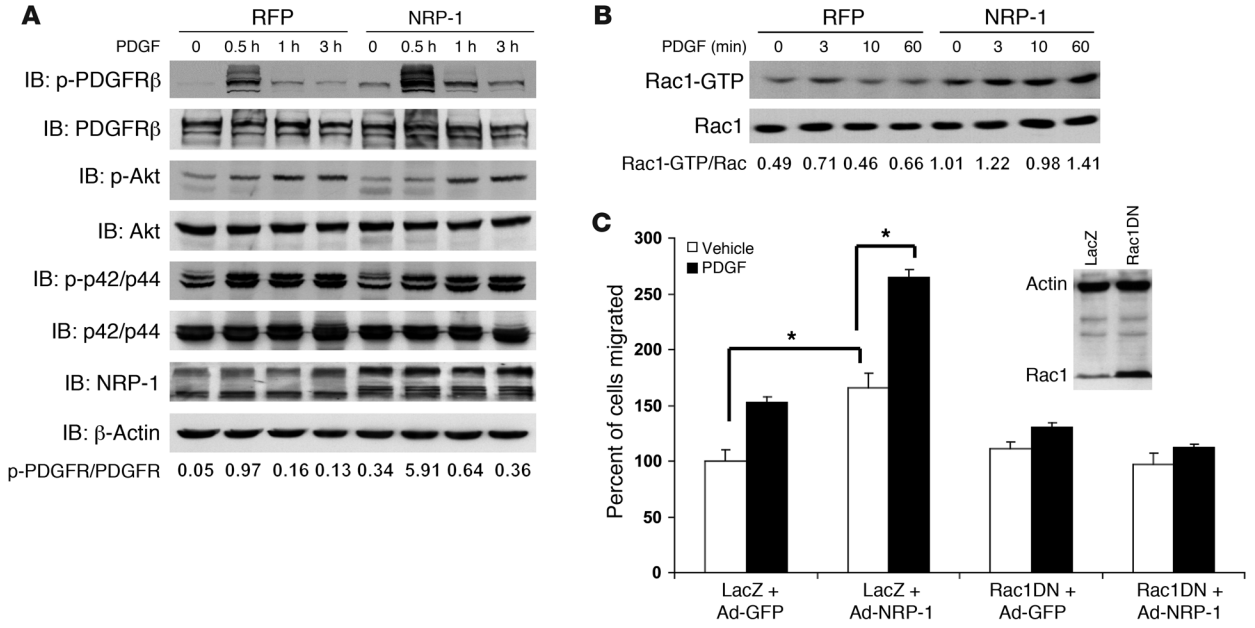

Figure 6

NRP-1 enhances PDGFRβ autophosphorylation and Rac1 activity. (**A**) hHSCs transduced with NRP-1–RFP or RFP alone were stimulated with PDGF-BB (10 ng/ml) for various durations of time from 0 to 180 minutes. Cell lysates were subjected to Western blot analyses with indicated Abs. NRP-1 overexpression enhanced the duration and intensity of PDGFRβ autophosphorylation at Tyr857. (**B**) Rac1 activity assay was performed with LX2 cells transduced with NRP-1–RFP and RFP and treated with PDGF-BB in a time series of 0, 3, 10, and 60 minutes. Rac1 activation levels are increased in LX2 cells transduced with NRP-1–RFP treated with PDGF-BB compared with HSCs transduced with RFP alone in the absence of changes in total Rac1 protein levels (representative autoradiographs or Western blots are from 3 independent experiments). (**C**) Rac1 inhibition blocks NRP-1–induced increase in cell migration. Ad–NRP-1 or Ad-GFP was cotransduced with a retroviral dominant negative Rac1 (Rac1DN) or LacZ in HSCs. Cell migration was analyzed in the presence of either vehicle or PDGF. The boxed Western blot shows the overexpression of Rac1DN in the experimental compared with the control group. *$P < 0.05$.

human HSCs and HSCs isolated from control rats or rats exposed to CCl_4. We examined two recently characterized NRP-1 Abs (NRP-1a and NRP-1b) (18) in these migration experiments and found that while both Abs showed inhibitory effects on PDGF-induced cell migration, NRP-1b showed a greater effect (Figure 8A), and we therefore used this Ab for all ensuing studies. As previously described, HSCs isolated from rats after CCl_4 exposure evidenced enhanced chemotaxis in response to PDGF (Figure 8B) (13, 34). Not only was chemotaxis further enhanced in these cells in response to NRP-1 overexpression, but more importantly, the enhanced PDGF-induced chemotaxis was markedly attenuated in response to incubation of cells with NRP-1b Ab (Figure 8B). This Ab inhibition effect was quantitatively comparable to that observed in mouse HSCs genetically depleted of NRP-1 (Supplemental Figure 9 shows the two data sets in juxtaposition). Similar results were obtained in an in vitro tubulogenesis assay, which correlates with angiogenic and fibrogenic phenotypes of liver HSCs in vivo (35) (Figure 8C).

We next returned to our in vivo liver models of HSC recruitment and myofibroblastic activation, which are characterized by excessive PDGFRβ activation, to test for a pathobiologic role of NRP-1 in this process using the NRP-1b Ab. Since enhanced HSC recruitment is one of the key determinants in development of liver fibrosis in vivo and a surrogate for the phenotype of HSC activation, we next examined whether NRP-1 is required for HSC/myofibroblast recruitment to sites of liver injury and fibrosis that occurs in mice in response to CCl_4 administration by systemically coadministering NRP-1b Ab. Interestingly, mice treated with CCl_4 and NRP-1b Ab evidenced a reduction in PDGFRβ- and NRP-1–positive HSCs (Figure 9A), corroborating the in vitro evidence of decreased HSC motility, migration, and tube formation. Additionally, Sirius red staining and hydroxyproline (a surrogate marker of collagen deposition) measurements revealed a reduction in fibrosis in mice receiving NRP-1b Ab in conjunction with CCl_4 (Figure 9A). *Pdgfrb* and *Nrp1* mRNA levels as assessed by qRT-PCR were also significantly reduced in mice treated with CCl_4 and NRP-1b Ab compared with CCl_4 alone (Figure 9B); mRNA levels of collagen1αI, α-*SMA*, *Tgfb*, *Ctgf*, and *Mmp3* — each a marker of hepatic fibrosis — evidenced a similar pattern of change (Figure 9C). *Timp1* induction was not reversed by NRP-1b Ab in vivo, providing specificity that not all potential targets are modified by NRP-1b Ab (Figure 9C).

Since in vivo liver injury models suggested that NRP-1 may promote HSC-driven matrix deposition in addition to promoting HSC recruitment, we next overexpressed NRP-1 in LX2 cells and treated them with PDGF-BB over a period ranging between 0 and 48 hours to examine the effects of NRP-1 on PDGF-induced collagen secretion. Indeed, although the canonical PDGF signal leads to migration rather than collagen deposition, HSCs overexpressing NRP-1 showed basal as well as PDGF-stimulated increases in collagen secretion, as quantified by Western blot analysis from concentrated culture medium from HSCs for type I collagen (Figure 10A). In a corroborative calorimetric assay, incubation of NRP-1–overexpressing HSCs with PDGF also significantly increased collagen deposition after 48 hours compared with control HSCs (Figure 10B).

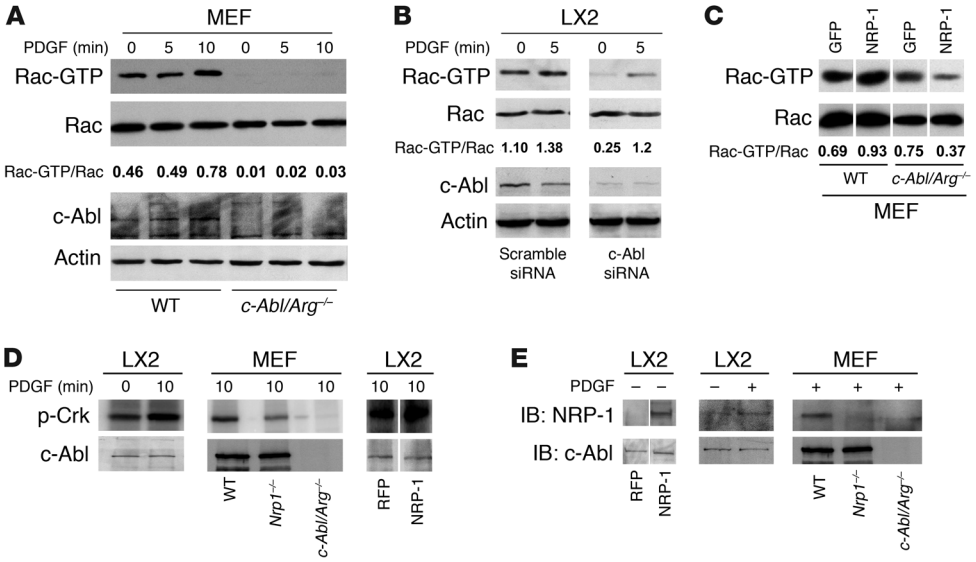

Figure 7

NRP-1 promotes Rac1 activity through c-Abl kinase activity. (**A**) Rac activity assay of *c-Abl/Arg*$^{-/-}$ MEFs was performed using GST-PBD pulldown assay after administration of PDGF (10 ng/ml) at different time points (0–10 minutes). Each group was analyzed by Western blot using Rac1 Ab. *c-Abl/Arg*$^{-/-}$ MEFs displayed impaired Rac1 activity. (**B**) siRNA knockdown of c-Abl was examined in LX2 cells incubated with vehicle or PDGF (10 ng/ml) for 5 minutes. Rac activity assay was performed from cell lysates and revealed reduced activity in cells transfected with c-Abl siRNA. Total Rac, c-Abl, and actin blots were performed on parallel, identically loaded membranes at the same time as GST pulldowns or autoradiography. (**C**) NRP-1 was overexpressed in wild-type or *c-Abl/Arg*$^{-/-}$ MEFs, and Rac1 activity was measured. Rac activity was markedly diminished in *c-Abl/Arg*$^{-/-}$ MEFs despite NRP-1 overexpression. (**D**) LX2 cells or MEFs (wild-type, *Nrp1*$^{-/-}$, *c-Abl/Arg*$^{-/-}$) were assessed for c-Abl activity in the presence or absence of PDGF. PDGF stimulation increased c-Abl activity in LX2 cells (left panel), and PDGF-induced c-Abl activity was impaired in MEFs isolated from *Nrp1*$^{-/-}$ MEFs (middle panel). Overexpression of NRP-1 enhanced c-Abl activity in the presence of PDGF (right panel). (**E**) Association of c-Abl and NRP-1 was assessed by coimmnuoprecipitation assay using c-Abl Ab. Binding of c-Abl and NRP-1 was enhanced in LX2 cells overexpressing NRP-1 (left panel). PDGF promoted binding of c-Abl and NRP-1 (middle panel). PDGF-induced binding was not detected in MEFs isolated from *c-Abl/Arg*$^{-/-}$ or *Nrp1*$^{-/-}$ MEFs (right panel). (**C**–**E**) Samples were run on the same membrane; noncontiguous lanes are denoted by white lines.

However, collagen secretion was markedly reduced from MEFs isolated from mice genetically deficient in c-Abl irrespective of NRP-1 overexpression (Figure 10C), indicating that c-Abl may be a key intermediary required for NRP-1 signal transduction. Thus, NRP-1 not only promotes PDGF-induced HSC migration but also amplifies a pathway of PDGF-induced collagen deposition.

Nonetheless, since TGF-β, rather than PDGFR, is thought to represent the canonical signal transducer for fibrosis in liver cirrhosis (36) and the effects of the neutralizing Ab in vivo were so prominent, we also investigated whether NRP-1 regulates TGF-β–induced collagen deposition. Indeed, NRP-1 overexpression in HSCs also promoted TGF-β–induced collagen secretion as assessed by Western blot and by a colorimetric assay (Figure 11, A and B). Furthermore, collagen deposition was markedly attenuated in MEFs isolated from NRP-1–deficient mice as well as from c-Abl–deficient mice (Figure 11C). Interestingly, NRP-1 overexpression did not further increase TGF-β–induced SMAD2 phosphorylation levels, further supporting a c-Abl–dependent and SMAD-independent mechanism of NRP-1 (data not shown). Finally, since VEGF-induced EC angiogenesis is a previously described regulatory target of NRP-1 (29), we also examined the role that the NRP-1 Ab may have on angiogenesis. Indeed, NRP-1 Ab reduced basal and VEGF-induced EC tubulogenesis (Supplemental Figure 8), substantiating the multitarget effects of NRP-1 Ab.

Last, we sought to correlate some of the aforementioned findings in the context of human cirrhosis. Samples of normal or cirrhotic liver of different stage and etiology were analyzed for NRP-1 expression by Western blot analysis and for histochemical analysis of fibrosis. NRP-1 expression was increased in cirrhotic liver lysates from patients with chronic hepatitis C in conjunction with increased expression of PDGFRβ, a molecule known to correlate with cirrhosis progression (34) (Figure 12A), and also correlated with fibrosis degree progression in patients with NASH (Figure 12B) — both liver diseases that are highly prevalent in the United States (37). These results were also corroborated at the mRNA level using qRT-PCR (Figure 12C). The most prominent increase, especially in NASH cirrhosis samples, was observed in the glycosylated form of NRP-1 (see 250-kDa band in Figure 12B), which is particularly relevant in light of studies demonstrating increased protein glycosylation in liver cirrhosis (38). Indeed, in retrospect, the presence of this glycosylated form of NRP-1 was also evident in activated HSCs such as LX2 cells in vitro (for example, Figure 2B and Figure 3, A and C).

Discussion

Liver cirrhosis is one of the 10 leading causes of mortality in the United States, with its vascular complication of portal hypertension accounting for the majority of morbidity and mortality (1). Outside of liver transplantation, treatment options are limited. This is worrisome, as some etiologies of cirrhosis such as hepatitis C– and NASH-based cirrhosis are highly prevalent (37). Research efforts aimed at developing new therapies have focused particularly on growth factor pathways that lead to activation of HSCs into myofibroblasts, especially the PDGF and TGF-β pathways (34, 39). Unfortunately, targeting these molecules on an individual basis has led to only limited therapeutic advance, highlighting the need to identify molecules that can concurrently target multiple growth factor signaling pathways (36). In this regard, the present data identify NRP-1 as a potential target for intervention in conditions typified by excessive activation of not only PDGFR and TGF-β, but also VEGF-induced angiogenesis, such as liver cirrhosis. Although it was first recognized as an axonal guidance molecule (40), the prominent effects of NRP-1 on vasculature became evident based

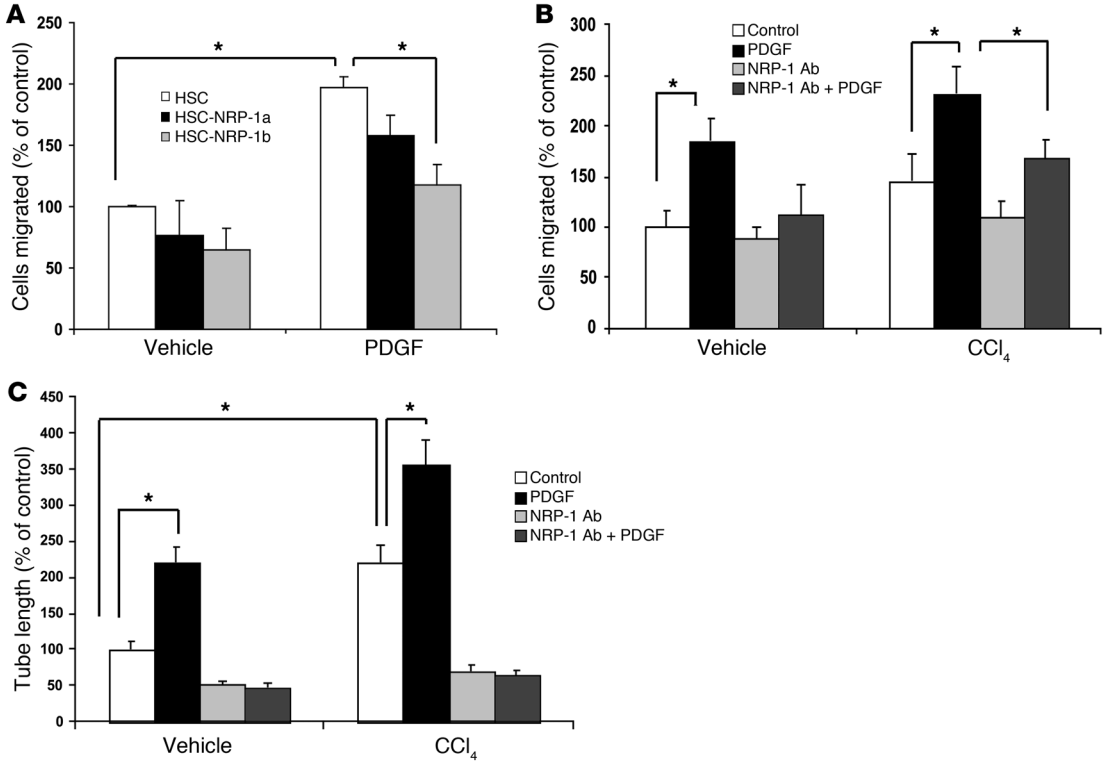

Figure 8

Ad NRP-1 increases the migratory and angiogenic phenotype of rHSCs from control and CCl_4-treated animals. (**A**) HSC migration was studied using Boyden chamber assay in the presence of 1 of 2 NRP-1–neutralizing Abs that bind to Sema-3A– (NRP-1a) or VEGF-binding (NRP-1b) domains of NRP-1, respectively. PDGF-induced HSC migration was more prominently affected by NRP-1b Ab than NRP-1a Ab ($n = 3$, $^*P < 0.05$). (**B**) Effect of NRP-1 Ab on PDGF-induced isolated rHSC migration using Boyden chamber was studied. NRP-1b Ab reduced PDGF-induced cell migration in rHSCs, nearly normalizing the enhanced motility observed in rHSCs isolated from CCl_4-treated rats ($n = 3$, $^*P < 0.05$). (**C**) NRP-1b Ab reduced the PDGF-induced tube formation ability of rHSCs isolated from rats treated with vehicle and/or CCl_4 and corrected the enhanced tube formation capacity of HSCs isolated from rats receiving CCl_4 ($n = 3$, $^*P < 0.05$).

on the changes observed in mice in response to genetic depletion and overexpression of *Nrp1* (16, 28). The phenotype was ascribed largely to EC-specific perturbation of VEGF signaling, since NRP-1 promotes VEGF signal transduction (16, 29, 41). However, recent studies suggesting that NRP-1 Ab could attenuate pericyte recruitment to tumors provided preliminary evidence that vascular wall cells other than ECs may also be a target for the actions of NRP-1 (18, 42). Thus, the present work is timely, since it highlights the sinusoidal HSC as an important target of NRP-1 in liver fibrosis.

In the present studies, NRP-1 overexpression not only increased the level and duration of PDGFRβ autophosphorylation in response to PDGF ligand, but also increased ligand-independent phosphorylation. NRP-1 overexpression also promoted Rac1 signaling downstream of PDGFRβ phosphorylation but not other canonical PDGFRβ-dependent targets such as ERK and Akt. These observations indicate that NRP-1 can also influence intracellular signaling independent of its extracellular coreceptor functions. Indeed, NRP-1 has a short, 40-amino-acid intracellular domain containing the SEA domain that is a putative signaling module by virtue of binding interactions with other intracellular adaptor proteins (43). For example, this domain has been proposed to mediate VEGF second messenger signaling in response to binding of VEGF with NRP-1 in ECs independent of other canonical VEGF receptors (29, 44), although the ability of NRP-1 to bind VEGF ligand independently of canonical VEGF receptors remains controversial (45). The effects of NRP-1 on PDGFR intracellular signaling suggest that NRP-1 can govern specificity of second messenger activation downstream from PDGFRβ phosphorylation in addition to its influence on ligand binding. This concept is further buttressed by our experimental evidence that NRP-1 signal selectivity is achieved by the non-receptor tyrosine kinase c-Abl, a model that is mechanistically distinct from that observed with NRP-1 regulation of VEGF signaling. Indeed, consistent with previous studies (46), we did not observe a prominent role of c-Abl in VEGF signaling in ECs (Supplemental Figure 3). c-Abl represents an ideal molecular relay, since this molecule has been previously demonstrated to link growth factor signaling with cell motility and collagen deposition by myofibroblasts (17). Indeed, modulation of c-Abl directly regulates both NRP-1 regulation of Rac1 activity as well as collagen deposition. Interestingly, c-Abl has been previously linked with both Rac1 activity and downstream cell motility and collagen deposition in myofibroblast cells by virtue of its ability to phosphorylate and activate the Rac1 GEF protein SOS-1 (33). Mechanistically, c-Abl binds NRP-1, and this binding is enhanced in response to growth factor activation and NRP-1 overexpression. Our proposed model of NRP-1 function in PDGFR signaling and the role of c-Abl is depicted schematically in Figure 13. It should be noted that this is a working model and that further studies will be necessary to

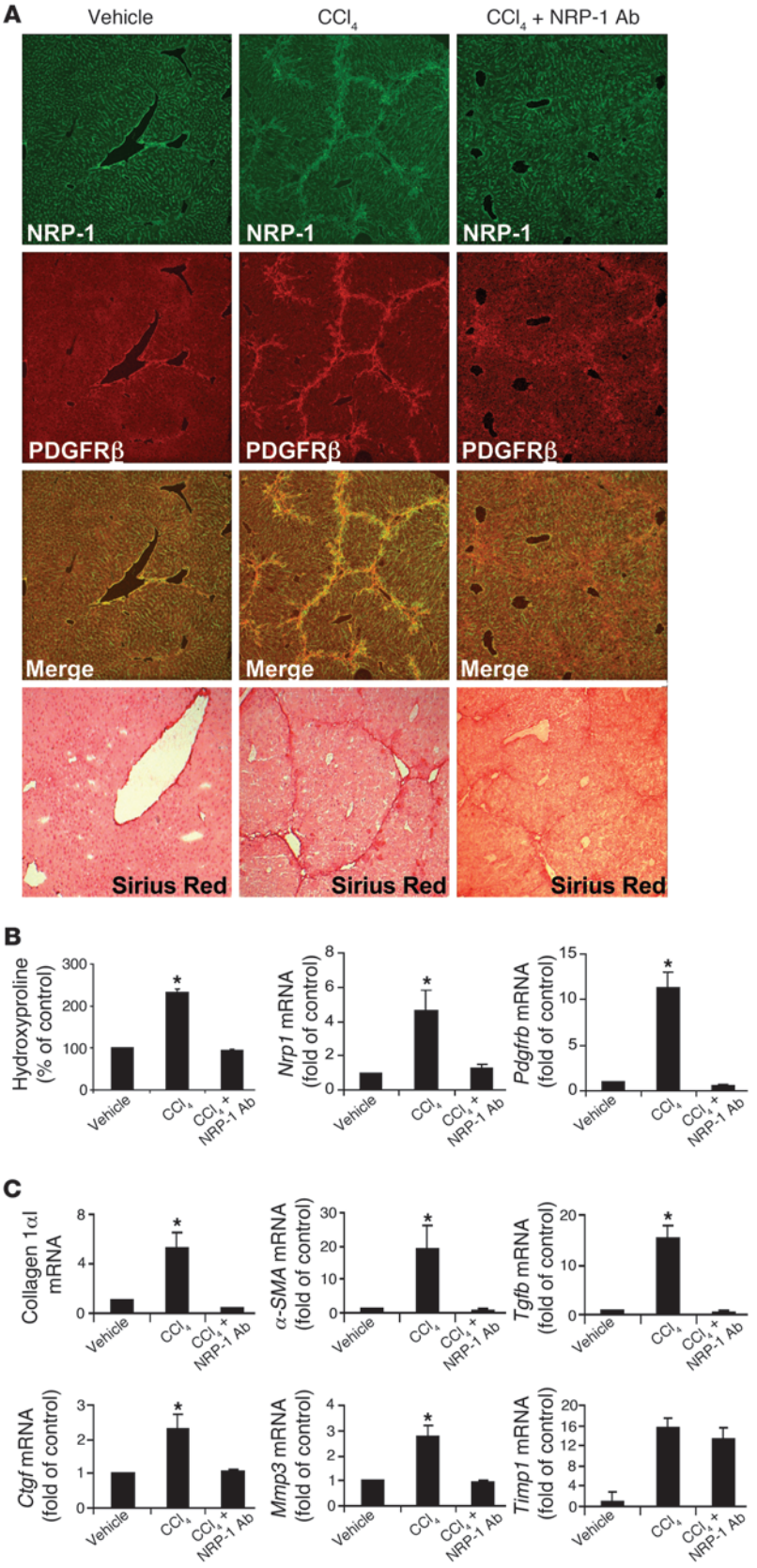

Figure 9
NRP-1 regulates PDGFRβ-dependent HSC functions in rodent cirrhosis in vivo. (**A**) Liver tissues of mice administered vehicle (n = 5), CCl_4 (n = 8) or CCl_4 in combination with i.p. injection of NRP-1b Ab (n = 8) were fixed and coimmunostained for PDGFRβ and NRP-1. Representative images for each staining show NRP-1 (green), PDGFRβ (red), and an overlay of the two (yellow). Liver sections of mice treated with vehicle, CCl_4, and CCl_4 with NRP-1 Ab were also stained with Sirius red to depict the fibrotic strands in red correlating with degree of fibrosis. Original magnification, ×10. (**B**) Hydroxyproline content was analyzed for the collagen estimation in liver of CCl_4-treated mice. Hydroxyproline levels were significantly reduced in mice treated with CCl_4 and NRP-1 Ab as compared with CCl_4 alone (n = 5–8, $^*P < 0.05$). *Pdgfrb* and *Nrp1* levels were quantified using qRT-PCR. The results from frozen tissue sections in each group showed that respective mRNA levels were significantly reduced in mice treated with CCl_4 and NRP-1 Ab compared with CCl_4 alone (n = 5–8, $^*P < 0.05$). (**C**) Collagen1αI, α-*SMA*, *Tgfb*, *Ctgf*, vimentin, *Mmp3*, and *Timp1* mRNA levels were quantified using qRT-PCR from the frozen tissue sections in each group. Results showed that collagen1αI, α-*SMA*, *Tgfb*, *Ctgf*, and *Mmp3* mRNA levels were significantly reduced in mice treated with CCl_4 and NRP-1 Ab compared with CCl_4 alone (n = 5–8, $^*P < 0.05$). *Timp1* mRNA levels remained unchanged in CCl_4-treated groups irrespective of NRP-1 Ab treatment.

definitively substantiate the basis by which NRP-1 directs PDGF signals selectively to Rac1 and not to ERK or Akt, especially since the enhanced PDGF binding conferred by NRP-1 could be expected to amplify all signals downstream from PDGFR.

In addition to the intracellular SEA domain, NRP-1 also contains larger extracellular protein domains. It is not yet resolved whether the extracellular domains of NRP-1 directly bind extracellular growth factor ligands or alternatively whether they enhance binding of specific growth factors to their cognate receptor (30, 40, 45, 47). Our present studies indicate that these two scenarios may not be mutually exclusive; while our ligand binding kinetic analyses demonstrate that NRP-1 increases the binding affinity of PDGF ligand with HSCs, the immunoprecipitation studies indicate that this occurs mostly through enhanced binding of PDGF with PDGFR, although some binding of ligand with NRP-1 was also detected upon NRP-1 overexpression. It is tempting to speculate that the recently characterized glycosaminoglycan side chains that decorate the extracellular portion of NRP-1 (45, 47–49) act as a "molecular net" that sequesters local PDGF ligand and funnels it towards its receptor. The close proximity of NRP-1 and PDGFR within low-buoyant-density membrane domains also supports such a model. It should be noted that such a model does not necessarily require direct binding between NRP-1 and PDGFRβ. Indeed, the direct binding of PDGFRβ and NRP-1 appears to be weak

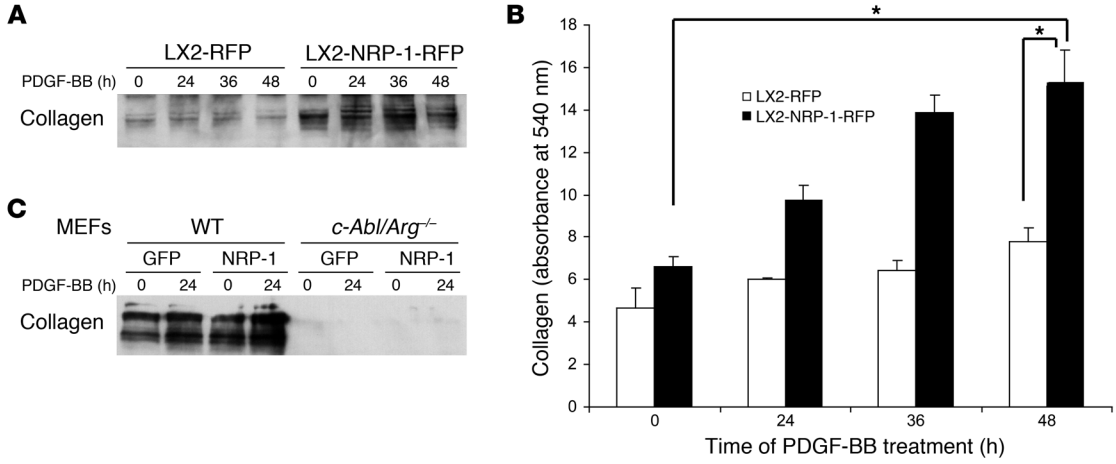

Figure 10
NRP-1 promotes PDGF-BB–induced collagen secretion in LX2 cells. LX2 cells or MEFs (wild-type or *c-Abl/Arg*$^{-/-}$) transduced with NRP-1–RFP or RFP alone were stimulated with PDGF-BB (10 ng/ml) for various durations of time from 0 to 48 hours after overnight serum starvation. (**A**) Media from cultured cells was collected, concentrated, and subjected to Western blot analysis for collagen I. NRP-1 overexpression promoted increased basal as well as PDGF-BB–induced collagen expression in LX2 cells ($n = 3$, with depiction of a representative radiograph). Membranes were stained with 0.5% Ponceau S, to assure equal protein loading (data not shown). (**B**) Total collagen content in the cell culture media was quantified using Sircol collagen assay. NRP-1 overexpression promoted basal as well as PDGF-BB–induced collagen secretion in LX2 cells ($n = 3$, $^*P < 0.05$). (**C**) Collagen I secretion was markedly reduced in *c-Abl/Arg*$^{-/-}$ compared with wild-type MEFs in the presence and absence or NRP-1 overexpression.

based on limited coprecipitation of the two proteins using Ab-based approaches (data not shown). Interestingly, this glycosylated form of NRP-1 was prominently increased in samples from patients with liver cirrhosis, as evidenced by the presence of a 250-kDa protein that was recognized by the NRP-1 Ab but was not reduced by excess reducing agent such as β-mercaptoethanol (data not shown). Interestingly, this higher-molecular-weight form was observed in human and murine HSCs but not in liver sinusoidal ECs (Supplemental Figure 6), providing further evidence that the increase in NRP-1 observed in our human cirrhotic samples is derived from HSCs, since the higher-molecular-weight form is prominently increased in the human cirrhotic samples (Figure 12). Indeed, a recent study suggests that glycosylation may be a protein mark conferred during the evolution of cirrhosis (38). Such approaches have even been proposed as a means to identify the level of liver fibrosis in individual patients (1).

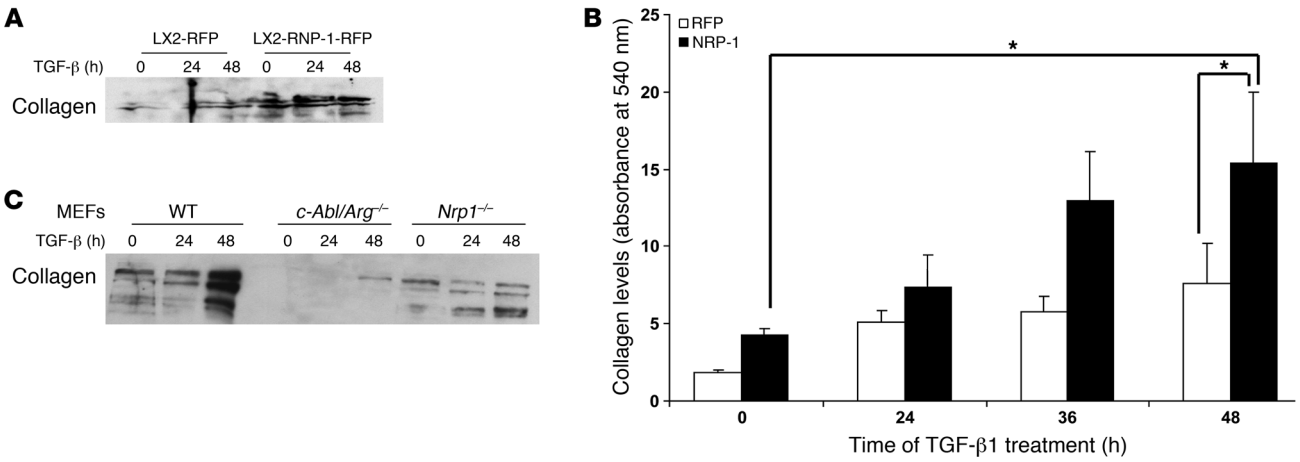

Figure 11
NRP-1 promotes TGF-β–induced collagen secretion in LX2 cells and MEFs. LX2 cells and MEFs (wild-type, *c-Abl/Arg*$^{-/-}$, and *Nrp1*$^{-/-}$) transduced with NRP-1 or RFP or GFP alone were stimulated with TGF-β (10 ng/ml) for various durations of time from 0 to 48 hours after overnight serum starvation. (**A**) Media from cultured cells was collected, concentrated, and subjected to Western blot analysis for collagen I. NRP-1 overexpression increased basal as well as TGF-β–induced collagen expression in LX2 cells ($n = 3$, with depiction of a representative radiograph). (**B**) Total collagen content in the cell culture media was quantified using Sircol collagen assay. NRP-1 overexpression promoted basal as well as TGF-β–induced collagen secretion in LX2 cells ($n = 3$, $^*P < 0.05$). (**C**) Media from cultured cells was collected and subjected to Western blot analysis for collagen I. NRP-1 overexpression promoted TGF-β–induced collagen secretion in MEFs, and deletion of *c-Abl* and *Nrp1* abrogated this effect.

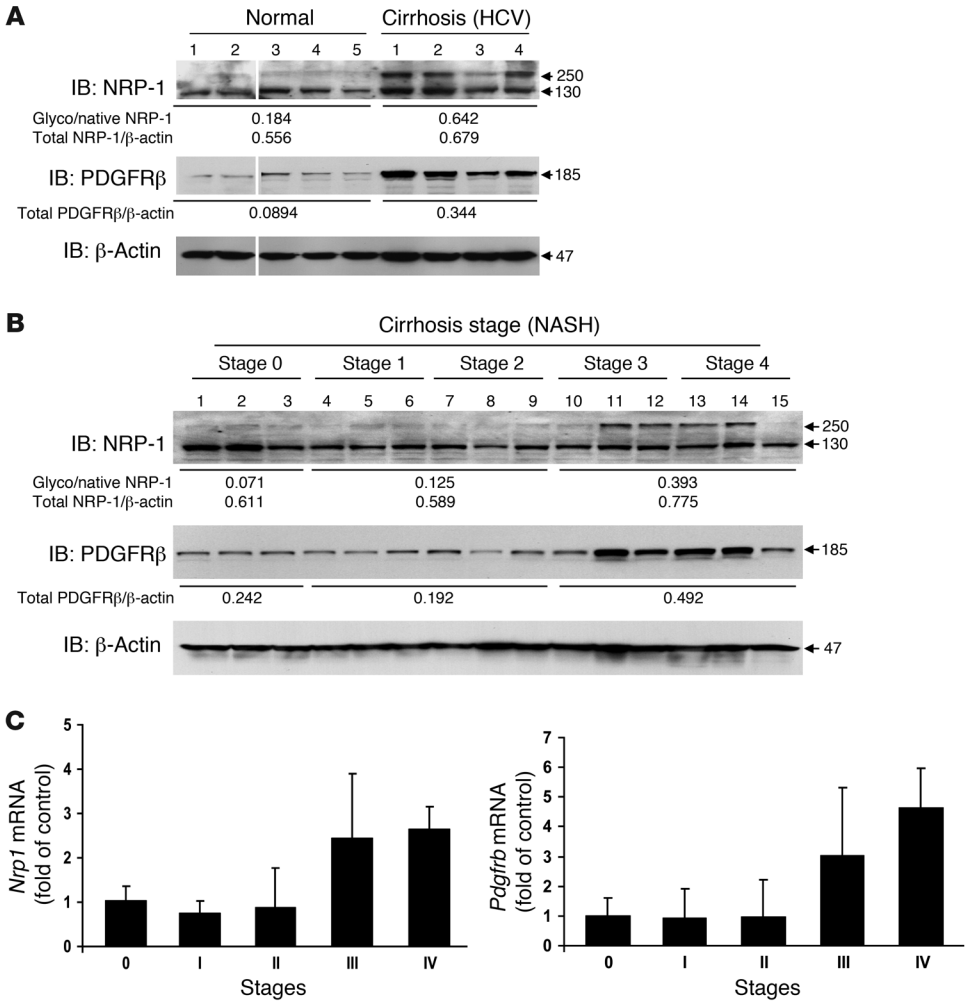

Figure 12
Increased NRP-1 expression in human cirrhotic specimens. (**A**) NRP-1 and PDGFRβ protein levels were increased in human cirrhotic liver (HCV) samples as assessed by Western blot analysis. Note the prominent increase in the higher-molecular-weight glycosylated form of NRP-1. The ratio of glycosylated/native (Glyco/native) NRP-1 and PDGFRβ/β-actin was increased in cirrhotic liver (HCV) samples compared with normal human liver samples. Samples were run on the same membrane; noncontiguous lanes are denoted by white lines. (**B**) NRP-1 and PDGFRβ protein levels were increased in correspondence with the stage of cirrhosis of human NASH liver samples. A similar increase in ratio of glycosylated/native NRP-1 and PDGFRβ/β-actin was observed with increasing stages of NASH samples (representative Western blots are from 3 independent experiments). (**C**) *Nrp1* and *Pdgfrb* mRNA levels were analyzed and compared in stage 0–4 human NASH liver samples. mRNA levels of both molecules were increased in human cirrhotic liver samples as assessed by qRT-PCR.

Angiogenesis is now increasingly linked to fibrosis, although the mechanistic relationship between these two processes is not fully defined (26, 35, 50). Since NRP-1 drives both angiogenesis in ECs (29) and both PDGF and TGF-β activation pathways in HSCs, targeting this molecule could have potentially synergistic effects on these linked processes that drive liver fibrosis. This could be an important benefit compared with other approaches currently under consideration, which have lacked adequately potent antifibrotic effects owing to the redundant pathways that drive liver fibrosis (36). Indeed, a human anti–NRP-1 Ab is under clinical evaluation in cancer, which is also frequently typified by both angiogenesis and prolific myofibroblast-derived fibrosis within the tumor microenvironment (51).

This current study builds on a stream of recent work that delineates parallel mechanisms of cell motility in pericytes and axonal guidance in neurons based on the premise that some forms of pericytes may derive embryologically from neuronal cells (35). HSCs also express ephrin family member proteins — another class of molecules that were initially characterized for their effects on neuronal repulsion prior to their identification as key regulators of HSC motility and tubulogenic capacity (35). NRP-1 was also originally identified as a regulator of neuronal growth cone collapse prior to evidence for its dominant role in angiogenesis (40). However, despite these parallels, some distinctions are evident in NRP-1 signal transduction in HSCs compared with neurons, with one notable example being the limited effects of the canonical neuronal NRP-1 ligand Sema3A within HSCs (Supplemental Figure 2D).

In summary, with the increasingly recognized pathophysiologic importance of HSCs in vivo, including their role in fibrosis and angiogenesis, we anticipate that these newly defined NRP-1 signaling pathways will be important for vascular structure and organ function relevant to liver cirrhosis. Particularly given the high prevalence of liver cirrhosis from NASH and HCV (37), development of new approaches to target HSCs for therapeutic benefit is of paramount importance. Furthermore, these observations may also be applicable to a diverse array of health and disease conditions associated with myofibroblast activation, desmoplasia, and fibrosis outside the liver as well.

Methods

Human subjects. Normal and cirrhotic liver samples obtained from biopsy and/or surgical waste under institutional review board–approved protocols were used for qRT-PCR, Western blot analysis, and/or histochemical studies.

Cell culture and transfection. HSCs isolated from mice, rats (rHSCs), and humans (hHSCs; ScienCell Research Laboratories) and LX2, a well-characterized cell line derived from human HSCs and human liver ECs (ScienCell Research Laboratories), were used in these studies as indicated in individual figure legends (52). PDGF-BB (Sigma-Aldrich), VEGF (R&D Systems),

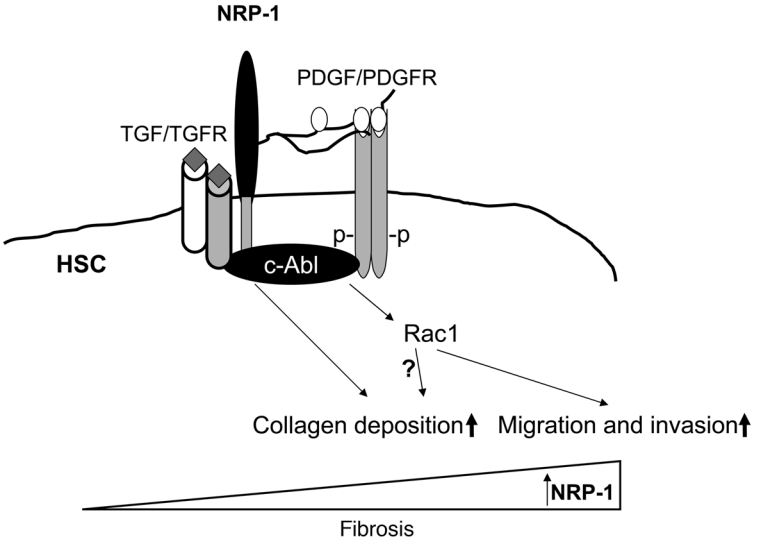

Figure 13
Mechanistic role of NRP-1 in liver fibrosis. A proposed model depicting the role of NRP-1 in liver fibrosis. NRP-1 increases PDGF ligand binding with PDGFR, thereby amplifying PDGFR phosphorylation. NRP-1 glycosylation chains are postulated to contribute to this process. NRP-1 also directs PDGFR signals toward Rac1 through its ability to bind and activate c-Abl, a protein that promotes Rac1 function. The intracellular SEA domain of NRP-1 may mediate this effect. NRP-1 also regulates other growth factors important for liver fibrosis including TGF-β and VEGF receptors in ECs (latter not shown). Increases in NRP-1 correspond with liver fibrosis progression and support this molecule as a potential therapeutic target for liver fibrosis treatment.

FGF (Sigma-Aldrich), and TGF-β (R&D Systems) were used at doses shown in individual figure legends. Cells were cultured in DMEM or specialized HSC medium, supplemented with 10% fetal bovine serum, 1 mmol/l L-glutamine, and 100 IU/ml streptomycin/penicillin. Adenoviral transduction of cells was performed as we described previously (52), using vectors encoding NRP-1–RFP or RFP control. Cells were incubated for 1 hour with 0.1% albumin/PBS with 50 MOI of adenoviruses encoding target genes, which achieved transduction efficiency approximating 90% with minimal toxicity in LX2 cells. For siRNA transfection, NRP-1 siRNA (200 nM; Dharmacon), c-Abl siRNA (50 nM; Santa Cruz Biotechnology Inc.), or appropriate control siRNA was transfected into LX2 cells, HSCs, or liver ECs by using Oligofectamine Reagent (Invitrogen). All assays were performed at the time points of 72–96 hours after transfection. Protein knockdown by siRNA was confirmed by Western blot analysis with specific Abs. MEFs were utilized in some experiments as indicated, where mice were embryonic lethal (*c-Abl/Arg*$^{-/-}$ MEFs; courtesy originally of Anthony Koleske, Yale University, New Haven, Connecticut, USA) or if use of murine HSCs was not feasible for the experimental protocol.

Murine HSCs. Murine HSCs used in these studies were isolated from *Nrp1* exon 2–floxed mice obtained from Alex Klotkin of John Hopkins University, Baltimore, Maryland, USA; originally generated by David Ginty's laboratory (28). Individual preps were prepared from pools of 3–4 mice to obtain adequate numbers of cells. All animal experiments were performed and mice maintained in compliance with protocols approved by the Mayo Clinic IACUC. Genotyping was performed as described previously (28). To confirm the loss of *Nrp1* in HSCs mediated by adenovirus Cre, we performed qRT-PCR on cDNA using primers targeting Nrp-exon 2 Fwd (5′-AACCCACATTTCGATTTGGA-3′) and Nrp-exon 3 Rev (5′-TTCATAGCGGATGGAAAACC-3′) yielding a 200-bp product in the adenovirus Cre–mediated deletion of *Nrp1* in HSCs. Thermocycling conditions consisted of 34 cycles of 94°C, 30 seconds; 58°C, 30 seconds; and 72°C, 30 seconds.

Subcloning. An NRP-1 cDNA construct was subcloned into retroviral expression vector pLNCX containing RFP tag using TA cloning (primers: NRP-1-FP-BamHI, 5′-GGGATCCATGGAGAGGGGGCTGCCGCTC-3′, NRP-1-RP-BamHI, 5′-GGATCCCATGCCTCCGAATAAGTACTCTG-3′) as an intermediate step (53). The whole insert was sequenced for confirmation.

Retrovirus generation and transduction. Retroviruses were produced from a 293T packaging cell line (53, 54). In brief, 293T cells were grown to 30%–40% confluence and cotransfected with pMD.MLV gag.pol, pMD.G, and pLNCX vectors containing the cDNA sequence of interest. Cell culture supernatant containing high-titer viruses was collected after 48 hours. For retroviral transduction, diluted retroviral conditioned medium (diluted at 1:4 with DMEM completed medium) was added to 30%–50% confluent LX2 cells or HSCs with Polybrene (8 μg/ml) as we have previously done (53). Experiments were performed using NRP-1–RFP, dominant negative Rac1, RFP, and LacZ retroviruses with efficiency approximating 90% at 72 hours after transduction.

Subcellular membrane fractionation and immunoblotting. To prepare caveolae membrane microdomains, 10 confluent T-175 flasks of LX2 cells were harvested and homogenized in cold buffer A (0.25 mol/l sucrose, 1 mmol/l EDTA, and 20 mmol/l tricine [pH 7.8]) and centrifuged at 1,000 *g* for 10 minutes, as we previously described (55). The supernatant was layered onto 30% Percoll and centrifuged at 84,000 *g* for 30 minutes. The plasma membrane fraction was collected and brought to a volume of 2 ml with buffer A. An aliquot of this fraction was assayed as the crude membrane fraction. The crude membrane fraction was sonicated 3 times for 30 seconds, resuspended in a 23% solution of OptiPrep, and then placed in a new centrifuge tube. A linear 20%–10% OptiPrep gradient was layered on top and centrifuged at 52,000 *g* for 90 minutes. Twelve 0.5-ml fractions were collected and analyzed via SDS-PAGE. Equal volumes of each membrane fraction were loaded (depicted on representative gel), and data were normalized for measured protein content (depicted in the accompanying graph). Efficiency of separation and purity of membrane fractions was determined by immunoblotting for caveolin-1 and β-COP, markers for caveolae and Golgi membrane fractions, respectively. For immunoblotting, protein lysates or specific subcellular fractions were heated to 60°C for 10 minutes in sample buffer containing 0.8 M DTT (Sigma-Aldrich) and 10% SDS (Fisher Scientific) for protein denaturation and solubilization. The samples were subjected to electrophoresis through 7.5% or 12% SDS-polyacrylamide gels and transferred overnight to nitrocellulose sheets. After blocking, the blots were incubated with anti–NRP-1 (Santa Cruz Biotechnology Inc.); this Ab recognizes human NRP-1 by Western blot but does not recognize rodent NRP-1 by Western blot. Other Abs included anti–phospho-PDGFRβ (Tyr857), anti-PDGFRβ, phospho-p44/42 MAPK (Thr202, Tyr204), p44/42 MAPK, Akt Ab, phospho-Akt (Ser473) (Cell Signaling Technology). The blots were washed and incubated for 1 hour at room temperature with appropriate secondary Abs. Protein bands were detected using an enhanced chemiluminescence detection system (ECL Plus; Amersham). After exposure of the nitrocellulose sheets to Kodak XAR film, the autoradiographs were scanned and quantified by densitometry using NIH Image software.

qRT-PCR. Real-time fluorescence monitoring was performed with the Applied Biosystems 7500 Real Time PCR System instrument as described previously (56). *Nrp1*, *Pdgfrb*, collagen1αI, α-*SMA*, *Tgfb*, *Ctgf*, *Mmp3*, or *Timp2* mRNA was normalized to *Gapdh* or β-actin mRNA, with results shown as fold change.

Confocal immunofluorescence microscopy. Liver tissues from CCl_4-treated, vehicle-treated, BDL, or sham-operated rats were harvested at varying times as indicated in figure legends and fixed in O.C.T. Sections (5-μm) were cut and mounted on slides. Samples were blocked with 10% goat serum in PBS for 1 hour and then incubated with goat anti–rat polyclonal NRP-1 Ab (1:10) and rabbit monoclonal PDGFRβ Ab (1:80) overnight at 4°C, followed by incubation for 1 hour with Alexa Fluor 488–conjugated donkey anti-goat (1:250) and Alexa Fluor 546–conjugated goat anti-rabbit (1:250) secondary Abs, respectively. The slides were then counterstained with DAPI, and confocal microscopy was performed by LSM 5 Pascal (Zeiss), in which appropriate laser and filter combinations were selected according to excitation and emission spectrum features of the Alexa fluorochromes. For cell microscopy, LX2 cells transduced with PDGFRβ retrovirus were seeded onto a Lab-Tek Chamber slide system (Nunc) cotransduced with Ad–NRP-1–RFP. Cells were washed and incubated with 2% paraformaldehyde solution for 10 minutes at room temperature. The primary Abs used in isolated cells were goat anti–human polyclonal NRP-1 Ab (1:50) and rabbit monoclonal PDGFRβ Ab (1:100). The secondary Abs used were Alexa Fluor 546–conjugated donkey anti-goat and Alexa Fluor 488–conjugated donkey anti-rabbit, respectively. Fluorescence was visualized with Zeiss LSM 5 Pascal, and images were processed with LSM image software.

Collagen secretion measurement. Total collagen was assessed in supernatants using the Sircol Soluble Collagen Assay kit (Accurate Scientific) according to the manufacturer's specifications. Briefly, media from the cultured cells was concentrated using Amicon Ultra (Millipore) centrifugal filter units, and 50 μl of each sample was transferred to a new tube. Sircol dye reagent (1.0 ml) was added and gently mixed for 30 minutes at room temperature. Samples were then centrifuged at 10,000 *g* for 10 minutes, the supernatant was discarded, and 1.0 ml of Sircol alkali reagent was then added to each sample and gently mixed until precipitates dissolved completely. Samples were introduced into spectrophotometer, and absorbance was read at 540 nm. Collagen secretion was also measured from concentrated supernatants by Western blot techniques described above and using anti–collagen type I Ab (600-401-103, Rockland).

Boyden chamber assay. Chemotaxis was measured by modified Boyden chamber assays (BD) with the use of 8-μm-pore-size polycarbonated filters coated with type I collagen (50 μg/ml) as described previously (56). Briefly, cells (LX2 cells and hHSCs) transduced with NRP-1–RFP or RFP retrovirus were suspended in serum-free medium and seeded to the upper wells (20,000 cells/well), while lower chambers were filled with 26 μl serum-free medium with 10 ng/ml of PDGF-BB, b-FGF (25 ng/ml), the PDGFR inhibitor imatinib (10 μmol/l), or vehicle as we have previously done (35). Isolated HSCs from rats treated with vehicle and/or CCl_4 preincubated with NRP-1b Ab (50 μg/ml) were also used in a separate set of experiments. Similar studies were done with human liver ECs transfected with c-Abl siRNA or scrambled siRNA with or without VEGF. After 4 hours incubation at 37°C, the polycarbonated filter was removed and migrated cells on the lower surface were stained with HEMA-3. Cells passed through the filter were quantified from random microscopic fields as we have previously done (52). Each assay was carried out in triplicate, with 6 replicates of each group per assay. Results are expressed as the mean number of migrated cells ± SEM.

Real-time video microscopy. Real-time video microscopy was conducted with a Zeiss confocal laser microscope equipped with an on-stage mini-chamber providing routine incubation conditions (37°C, 5% CO_2). Differential interference contrast (DIC) and fluorescence images of cells were taken in 90- and 180-second intervals using a CCD C2400 camera (Hamamatsu Photonics K.K.). We used hHSCs transfected with Cy3-labeled siRNA of NRP-1 or scrambled siRNA as control. Alternatively, cells were transduced with RFP control or NRP-1–RFP retrovirus for analysis. Image processing and data analysis were performed using MetaMorph (Universal Imaging/Molecular Devices) software and the data (distance [μm] or velocity [μm/s]) were transferred to Excel (Microsoft) for analysis and graphing. For video display, image stacks were compressed and processed as Media Player movies (Microsoft). Sixty images were recorded for each single experiment, with time intervals between the images of 90 seconds. Semiautomated extraction of the video sequences by MetaMorph Imaging System was performed. For cell migration analysis, a number of randomly selected cells from several videos were tracked using the track point function of MetaMorph Imaging to determine cell trajectories and distance covered by each cell over the period of time. Fluorescently labeled cells were tracked using the track object function in MetaMorph Imaging.

Wound healing assay. Serum-starved confluent cell monolayers were scratch wounded using a 200-μl pipette tip to induce migration into the wound. Cells overexpressing NRP-1–RFP and control cells were treated with either vehicle or recombinant PDGF-BB (10 ng/ml). Cells were tracked at the wound edge for 6 hours using time-lapse movies. For quantification of cell migration, we used MetaMorph Imaging software as described previously (57).

Vascular tube formation assay. Cells were placed on 100 μl Matrigel after 30 minutes of preincubation at 37°C. Primary rHSCs isolated from vehicle- or CCl_4-treated rats were transduced with Ad–NRP-1 to overexpress NRP-1 or Ad-GFP as control. Cells were washed, trypsinized, and seeded at 2×10^4 cells/well on Matrigel Matrix–coated (BD Biosciences) chamber slides. Cells were incubated in the presence of either vehicle or 10 nM PDGF for 12–18 hours at 37°C and 5% CO_2 and imaged using a ×4 objective lens and analyzed using Image-Pro Plus software (Media Cybernetics) for quantification of tube formation as described previously (35). Experiments with liver ECs were performed in the presence and absence of exogenous VEGF (10 ng/ml) and or NRP-1b Ab (50 μg/ml). In addition, similar experiments were done with liver ECs transfected with c-Abl siRNA and scrambled siRNA.

Rac1 GST pulldown assay. GST-agarose beads bound to a portion of p21-activated kinase (PAK-1) containing amino acids 74–89 of the N-terminal regulatory region (p21-binding domain [PBD]) were added to the cell lysates (10 μl beads for every 500 μg cell lysate in 500 μl). Following incubation, beads were washed, and bound proteins were eluted with loading buffer and analyzed by SDS-PAGE/Western blot using anti-Rac1 Ab. The activity of Rac1 was determined at the indicated time points after PDGF incubation (52).

Ligand binding and cross-linking assays. Recombinant PDGF-BB (10 μg; Sigma-Aldrich) was dissolved in 200 μl 4-mM HCl and mixed with 5 mCi $Na^{125}I$ (Amersham Pharmacia Biotech). The iodine/protein mixture was then mixed with CIT (chloramine T; 100 μl; 1 μg/μl) and incubated 2 minutes on ice, and then the iodination was stopped by 100 μl sodium hydrogen sulfite ($Na_2S_2O_5$, 5 μg/μl). The iodinated protein was then dialyzed 3 times against 1 l dialysis buffer (10 mM acetic acid, 150 mM NaCl) over a period of 2–3 days to separate unincorporated ^{125}I. The labeled protein had a final specific activity of 5.0×10^4 cpm ng^{-1}. Cells were plated into 24-well tissue culture dishes and cultured for 3 days. Cells were washed once with ice-cold binding buffer (DMEM/F-12 containing 0.1% bovine serum albumin, 20 mM HEPES, pH 7.2) and then incubated with ^{125}I–PDGF-BB (250 pM) diluted in binding buffer. The samples were incubated for 2 hours on ice and washed 3 times with binding buffer, and the bound counts were harvested by the addition of extraction buffer (1% Triton X-100, Sigma-Aldrich). The extracts were counted in a gamma counter to determine total level of ^{125}I–PDGF-BB bound. For receptor competition assays, cells were cultured in 24-well plates and incubated with ^{125}I–PDGF-BB in the presence of increasing amounts of PDGF-BB (100–400 pM). Binding, washing,

and extraction conditions for these experiments were similar to those used for the above ligand-binding experiments. For cross-linking studies, cells were incubated with 250 pM ^{125}I–PDGF-BB for 2 hours on ice. Following a wash, receptor-ligand complexes were cross-linked by incubating cells in 3 mM bis(sulfosuccinimidyl) suberate (Pierce) for 30 minutes on ice, and the reaction was quenched by rinsing cells in Tris-buffered saline. Cells were extracted in lysis buffer and lysates precleared with protein A–agarose beads. Cell extracts were subjected to immunoprecipitation with 4 μg of either anti-PDGFRβ or anti–NRP-1 and normal mouse or goat IgG as control for 1.5 hours at room temperature, followed by incubation with protein A–agarose beads for 2 hours at room temperature. Beads were collected through centrifugation, rinsed 3 times in PBS plus 0.1% bovine serum albumin, and boiled for 5 minutes in 50 μl reducing sample buffer. Samples were run on a 7.5% Tris-SDS-PAGE, and the dried gel was exposed to film for 1 week.

C-Abl kinase assay. In vitro kinase assays were performed as described in previous studies (17). In brief, c-Abl protein was immunoprecipitated from extracts of cells treated experimentally as described in individual experiments. The immunoprecipitates were washed, and kinase reactions were performed for 20 minutes at 25°C after adding 1 μg of GST-Crk substrate, 100 μM cold ATP, and 5 μCi [^{32}P]-γ-ATP. Samples were separated by SDS-PAGE and analyzed by autoradiography with a Storm PhosphorImager system.

Cirrhotic animal models and histological analysis. Rats were administered CCl_4 (0.5 mg/kg) or olive oil vehicle for 6 weeks, i.p. Cirrhosis was also induced by BDL as previously described (34, 35). Animals were sacrificed and primary rHSCs isolated as described previously. In a separate set of experiments, mice were similarly administered CCl_4 (0.5 mg/kg) or olive oil vehicle for 6 weeks in the presence of either NRP-1 Ab (10 mg/kg) or vehicle, i.p. Liver was harvested for expression of fibrosis markers using qRT-PCR (56) and histological analysis (35) as described previously.

Proliferation assay. The relative proliferation rates of LX2 cells transduced with RFP or NRP-1–RFP retrovirus were determined by MTS assay on 96-well plates as described previously (58).

Statistics. Experiments were performed at least 3 independent times and numerical data expressed as mean ± SEM. The significance of the differences of the means was evaluated by paired and unpaired 2-tailed Student's *t* test or ANOVA as appropriate. A *P* value less than 0.05 was considered significant.

Acknowledgments

We are grateful to Daniel Dimaio (Yale University) for providing the PDGFRβ cDNA, Geoff L. Curran for ^{125}I labeling assistance, and Kim Viker for assistance with human samples. This work was supported by NIH grants R01 DK 59615 and R01 HL 86990 (to V.H. Shah) and P30 DK 084567 — Clinical Core; American Heart Association Scientist Development Grant AHA0435063N (to S. Cao); and a Pilot and Feasibility Award from the Mayo Clinic Center on Cell Signaling in Gastroenterology (to A. Das).

Received for publication January 7, 2010, and accepted in revised form May 5, 2010.

Address correspondence to: Vijay Shah or Sheng Cao, Mayo Clinic, 200 First ST SW, Rochester, Minnesota 55905, USA. Phone: 507.255.6028 (V. Shah) or 507.538.7641 (S. Cao); Fax: 507.255.6318; E-mail: shah.vijay@mayo.edu (V. Shah) or cao.sheng@mayo.edu (S. Cao).

1. Schuppan D, Afdhal NH. Liver cirrhosis. *Lancet*. 2008;371(9615):838–851.
2. Shah VH, Kamath PS. Portal hypertension and gastrointestinal bleeding. In Feldman M, Friedman LS, Brandt LJ, eds. *Sleisenger and Fordtran's Gastrointestinal and Liver Disease*. 8th ed. Philadelphia, Pennsylvania, USA: Elsevier Health Sciences; 2006:1899–1934.
3. Friedman SL. Mechanisms of hepatic fibrogenesis. *Gastroenterology*. 2008;134(6):1655–1669.
4. Rockey DC. Current and future anti-fibrotic therapies for chronic liver disease. *Clin Liver Dis*. 2008; 12(4):939–962.
5. Jain R, Booth M. What brings pericytes to tumor vessels? *J Clin Invest*. 2003;112(8):1134–1136.
6. Lee JS, Semela D, Iredale J, Shah VH. Sinusoidal remodeling and angiogenesis: a new function for the liver-specific pericyte? *Hepatology*. 2007; 45(3):817–825.
7. Claesson-Welsh L, et al. cDNA cloning and expression of a human platelet-derived growth factor (PDGF) receptor specific for B-chain-containing PDGF molecules. *Mol Cell Biol*. 1988;8(8):3476–3486.
8. Westermark B, Siegbahn A, Heldin CH, Claesson-Welsh L. B-type receptor for platelet-derived growth factor mediates a chemotactic response by means of ligand-induced activation of the receptor protein-tyrosine kinase. *Proc Natl Acad Sci U S A*. 1990; 87(1):128–132.
9. Lai CC, Henningson C, DiMaio D. Bovine papillomavirus E5 protein induces oligomerization and trans-phosphorylation of the platelet-derived growth factor beta receptor. *Proc Natl Acad Sci U S A*. 1998;95(26):15241–15246.
10. Soriano P. Abnormal kidney development and hematological disorders in PDGF beta-receptor mutant mice. *Genes Dev*. 1994;8(16):1888–1896.
11. Abramsson A, Lindblom P, Betsholtz C. Endothelial and nonendothelial sources of PDGF-B regulate pericyte recruitment and influence vascular pattern formation in tumors. *J Clin Invest*. 2003; 112(8):1142–1151.
12. Lindblom P, et al. Endothelial PDGF-B retention is required for proper investment of pericytes in the microvessel wall. *Genes Dev*. 2003;17(15):1835–1840.
13. Wong L, Yamasaki G, Johnson RJ, Friedman SL. Induction of beta-platelet-derived growth factor receptor in rat hepatic lipocytes during cellular activation in vivo and in culture. *J Clin Invest*. 1994; 94(4):1563–1569.
14. Friedman SL, Arthur MJ. Activation of cultured rat hepatic lipocytes by Kupffer cell conditioned medium. Direct enhancement of matrix synthesis and stimulation of cell proliferation via induction of platelet-derived growth factor receptors. *J Clin Invest*. 1989;84(6):1780–1785.
15. Iredale JP. Models of liver fibrosis: exploring the dynamic nature of inflammation and repair in a solid organ. *J Clin Invest*. 2007;117(3):539–548.
16. Kawasaki T, et al. A requirement for neuropilin-1 in embryonic vessel formation. *Development*. 1999; 126(21):4895–4902.
17. Daniels C, et al. Imatinib mesylate inhibits the profibrogenic activity of TGF-beta and prevents bleomycin-mediated lung fibrosis. *J Clin Invest*. 2004; 114(9):1308–1316.
18. Pan Q, et al. Blocking neuropilin-1 function has an additive effect with anti-VEGF to inhibit tumor growth. *Cancer Cell*. 2007;11(1):53–67.
19. Sancho-Bru P, et al. Genomic and functional characterization of stellate cells isolated from human cirrhotic livers. *J Hepatol*. 2005;43(2):272–282.
20. Hellerbrand C, Stefanovic B, Giordano F, Burchardt ER, Brenner DA. The role of TGFbeta1 in initiating hepatic stellate cell activation in vivo. *J Hepatol*. 1999;30(1):77–87.
21. Xu L, et al. Human hepatic stellate cell lines, LX-1 and LX-2: new tools for analysis of hepatic fibrosis. *Gut*. 2005;54(1):142–151.
22. Liu P, Ying Y, Ko YG, Anderson RG. Localization of platelet-derived growth factor-stimulated phosphorylation cascade to caveolae. *J Biol Chem*. 1996;271(17):10299–10303.
23. Veracini L, Franco M, Boureux A, Simon V, Roche S, Benistant C. Two distinct pools of Src family tyrosine kinases regulate PDGF-induced DNA synthesis and actin dorsal ruffles. *J Cell Sci*. 2006; 119(pt 14):2921–2934.
24. Beardsley A, Fang K, Mertz H, Castranova V, Friend S, Liu J. Loss of caveolin-1 polarity impedes endothelial cell polarization and directional movement. *J Biol Chem*. 2005;280(5):3541–3547.
25. Greenberg JI, et al. A role for VEGF as a negative regulator of pericyte function and vessel maturation. *Nature*. 2008;456(7223):809–813.
26. Novo E, et al. Proangiogenic cytokines as hypoxia-dependent factors stimulating migration of human hepatic stellate cells. *Am J Pathol*. 2007; 170(6):1942–1953.
27. Liu W, et al. Upregulation of neuropilin-1 by basic fibroblast growth factor enhances vascular smooth muscle cell migration in response to VEGF. *Cytokine*. 2005;32(5):206–212.
28. Gu C, et al. Neuropilin-1 conveys semaphorin and VEGF signaling during neural and cardiovascular development. *Dev Cell*. 2003;5(1):45–57.
29. Wang L, Zeng H, Wang P, Soker S, Mukhopadhyay D. Neuropilin-1-mediated vascular permeability factor/vascular endothelial growth factor-dependent endothelial cell migration. *J Biol Chem*. 2003;278(49):48848–48860.
30. Soker S, Takashima S, Miao HQ, Neufeld G, Klagsbrun M. Neuropilin-1 is expressed by endothelial and tumor cells as an isoform-specific receptor for vascular endothelial growth factor. *Cell*. 1998;92(6):735–745.
31. Andrae J, Gallini R, Betsholtz C. Role of platelet-derived growth factors in physiology and medicine. *Genes Dev*. 2008;22(10):1276–1312.
32. De Donatis A, et al. Proliferation versus migra-

tion in platelet-derived growth factor signaling: the key role of endocytosis. *J Biol Chem*. 2008; 283(29):19948–19956.
33. Sini P, Cannas A, Koleske AJ, Di Fiore PP, Scita G. Abl-dependent tyrosine phosphorylation of Sos-1 mediates growth-factor-induced Rac activation. *Nat Cell Biol*. 2004;6(3):268–274.
34. Rockey DC, Housset CN, Friedman SL. Activation-dependent contractility of rat hepatic lipocytes in culture and in vivo. *J Clin Invest*. 1993;92(4):1795–1804.
35. Semela D, Das A, Langer DA, Kang N, Leof E, Shah VH. Platelet-derived growth factor signaling through ephrin-B2 regulates hepatic vascular structure and function *Gastroenterology*. 2008;135(2):671–679.
36. Bataller R, Brenner DA. Liver fibrosis. *J Clin Invest*. 2005;115(2):209–218.
37. Kim WR, Brown RS Jr, Terrault NA, El-Serag H. Burden of liver disease in the United States: summary of a workshop. *Hepatology*. 2002;36(1):227–242.
38. Callewaert N, Van Vlierberghe H, Van Hecke A, Laroy W, Delanghe J, Contreras R. Noninvasive diagnosis of liver cirrhosis using DNA sequencer-based total serum protein glycomics. *Nat Med*. 2004; 10(4):429–434.
39. Friedman SL. Reversibility of hepatic fibrosis and cirrhosis--is it all hype? *Nat Clin Pract Gastroenterol Hepatol*. 2007;4(5):236–237.
40. He Z, Tessier-Lavigne M. Neuropilin is a receptor for the axonal chemorepellent Semaphorin III. *Cell*. 1997; 90(4):739–751.
41. Bates D, et al. Neurovascular congruence results from a shared patterning mechanism that utilizes Semaphorin3A and Neuropilin-1. *Dev Biol*. 2003; 255(1):77–98.
42. Banerjee S, et al. Breast cancer cells secreted platelet-derived growth factor-induced motility of vascular smooth muscle cells is mediated through neuropilin-1. *Mol Carcinog*. 2006;45(11):871–880.
43. Cai H, Reed RR. Cloning and characterization of neuropilin-1-interacting protein: a PSD-95/Dlg/ZO-1 domain-containing protein that interacts with the cytoplasmic domain of neuropilin-1. *J Neurosci*. 1999;19(15):6519–6527.
44. Prahst C, et al. Neuropilin-1-VEGFR-2 complexing requires the PDZ-binding domain of neuropilin-1. *J Biol Chem*. 2008;283(37):25110–25114.
45. Kawamura H, et al. Neuropilin-1 in regulation of VEGF-induced activation of p38MAPK and endothelial cell organization. *Blood*. 2008; 112(9):3638–3649.
46. Yan W, Bentley B, Shao R. Distinct angiogenic mediators are required for basic fibroblast growth factor- and vascular endothelial growth factor-induced angiogenesis: the role of cytoplasmic tyrosine kinase c-Abl in tumor angiogenesis. *Mol Biol Cell*. 2008;19(5):2278–2288.
47. Klagsbrun M, Takashima S, Mamluk R. The role of neuropilin in vascular and tumor biology. *Adv Exp Med Biol*. 2002;515:33–48.
48. Shintani Y, et al. Glycosaminoglycan modification of neuropilin-1 modulates VEGFR2 signaling. *EMBO J*. 2006;25(13):3045–3055.
49. Frankel P, et al. Chondroitin sulphate-modified neuropilin 1 is expressed in human tumour cells and modulates 3D invasion in the U87MG human glioblastoma cell line through a p130Cas-mediated pathway. *EMBO Rep*. 2008;9(10):983–989.
50. Taura K, et al. Hepatic stellate cells secrete angiopoietin 1 that induces angiogenesis in liver fibrosis. *Gastroenterology*. 2008;135(5):1729–1738.
51. Kalluri R, Zeisberg M. Fibroblasts in cancer. *Nat Rev Cancer*. 2006;6(5):392–401.
52. Lee J, Decker N, Chatterjee S, Yao J, Friedman S, Shah V. Mechanisms of nitric oxide interplay with Rho GTPase family members in modulation of actin membrane dynamics in pericytes and fibroblasts. *Am J Pathol*. 2005;166(6):1861–1870.
53. Kang-Decker N, et al. Nitric oxide promotes endothelial cell survival signaling through S-nitrosylation and activation of dynamin-2. *J Cell Sci*. 2007; 120(pt 3):492–501.
54. Zeng H, Zhao D, Mukhopadhyay D. KDR stimulates endothelial cell migration through heterotrimeric G protein Gq/11-mediated activation of a small GTPase RhoA. *J Biol Chem*. 2002;277(48):46791–46798.
55. Chatterjee S, Cao S, Petersen T, Simari R, Shah V. Inhibition of GTP-dependent vesicle trafficking impairs internalization of plasmalemmal eNOS and cellular nitric oxide production. *J Cell Sci*. 2003;116(pt 17):3645–3655.
56. Das A, et al. Disruption of an SP2/KLF6 Repression complex by SHP is required for farnesoid X receptor-induced endothelial cell migration. *J Biol Chem*. 2006;281(51):39105–39113.
57. Prigozhina NL, Waterman-Storer CM. Decreased polarity and increased random motility in PtK1 epithelial cells correlate with inhibition of endosomal recycling. *J Cell Sci*. 2006;119(pt 17):3571–3582.
58. Langer D, et al. Nitric oxide promotes caspase independent hepatic stellate cell apoptosis through generation of reactive oxygen species. *Hepatology*. 2008;47(6):1983–1993.